

# Northumbria Research Link

Citation: Woodham, L. D., Wicks, Robert, Verscharen, D., TenBarge, J. M. and Howes, G. G. (2021) Dependence of Solar Wind Proton Temperature on the Polarization Properties of Alfvénic Fluctuations at Ion-kinetic Scales. *The Astrophysical Journal*, 912 (2). p. 101. ISSN 0004-637X

Published by: IOP Publishing

URL: <https://doi.org/10.3847/1538-4357/abed51> <<https://doi.org/10.3847/1538-4357/abed51>>

This version was downloaded from Northumbria Research Link:  
<http://nrl.northumbria.ac.uk/id/eprint/46326/>

Northumbria University has developed Northumbria Research Link (NRL) to enable users to access the University's research output. Copyright © and moral rights for items on NRL are retained by the individual author(s) and/or other copyright owners. Single copies of full items can be reproduced, displayed or performed, and given to third parties in any format or medium for personal research or study, educational, or not-for-profit purposes without prior permission or charge, provided the authors, title and full bibliographic details are given, as well as a hyperlink and/or URL to the original metadata page. The content must not be changed in any way. Full items must not be sold commercially in any format or medium without formal permission of the copyright holder. The full policy is available online: <http://nrl.northumbria.ac.uk/policies.html>

This document may differ from the final, published version of the research and has been made available online in accordance with publisher policies. To read and/or cite from the published version of the research, please visit the publisher's website (a subscription may be required.)

3 DEPENDENCE OF SOLAR WIND PROTON TEMPERATURE ON THE POLARISATION PROPERTIES  
4 OF ALFVÉNIC FLUCTUATIONS AT ION-KINETIC SCALES

5 L. D. WOODHAM,<sup>\*,1</sup> R. T. WICKS,<sup>2,3,4</sup> D. VERSCHAREN,<sup>3,5</sup> J. M. TENBARGE,<sup>6,7</sup> & G. G. HOWES<sup>8</sup>

6 <sup>1</sup>Department of Physics, The Blackett Laboratory, Imperial College London, London, SW7 2AZ, UK

7 <sup>2</sup>Department of Mathematics, Physics & Electrical Engineering, Northumbria University, Newcastle upon Tyne, NE1 8ST, UK

8 <sup>3</sup>Mullard Space Science Laboratory, University College London, Holmbury St. Mary, Surrey RH5 6NT, UK

9 <sup>4</sup>Institute of Risk and Disaster Reduction, University College London, London, WC1E 6BT, UK

10 <sup>5</sup>Space Science Center, University of New Hampshire, Durham, NH 03824, USA

11 <sup>6</sup>Department of Astrophysical Sciences, Princeton University, Princeton, NJ 08544, USA

12 <sup>7</sup>Princeton Plasma Physics Laboratory, Princeton, NJ 08540, USA

13 <sup>8</sup>Department of Physics and Astronomy, University of Iowa, Iowa City, IA 52242, USA

14 *Draft version March 8, 2021*

15 ABSTRACT

16 We use fluctuating magnetic helicity to investigate the polarisation properties of Alfvénic fluctuations at ion-  
17 kinetic scales in the solar wind as a function of  $\beta_p$ , the ratio of proton thermal pressure to magnetic pressure,  
18 and  $\theta_{vB}$ , the angle between the proton flow and local mean magnetic field,  $\mathbf{B}_0$ . Using almost 15 years of *Wind*  
19 observations, we separate the contributions to helicity from fluctuations with wave-vectors,  $\mathbf{k}$ , quasi-parallel  
20 and oblique to  $\mathbf{B}_0$ , finding that the helicity of Alfvénic fluctuations is consistent with predictions from linear  
21 Vlasov theory. This result suggests that the non-linear turbulent fluctuations at these scales share at least some  
22 polarisation properties with Alfvén waves. We also investigate the dependence of proton temperature in the  
23  $\beta_p$ - $\theta_{vB}$  plane to probe for possible signatures of turbulent dissipation, finding that it correlates with  $\theta_{vB}$ . The  
24 proton temperature parallel to  $\mathbf{B}_0$  is higher in the parameter space where we measure the helicity of right-  
25 handed Alfvénic fluctuations, and the temperature perpendicular to  $\mathbf{B}_0$  is higher where we measure left-handed  
26 fluctuations. This finding is inconsistent with the general assumption that by sampling different  $\theta_{vB}$  in the solar  
27 wind we can analyse the dependence of the turbulence distribution on  $\theta_{kB}$ , the angle between  $\mathbf{k}$  and  $\mathbf{B}_0$ . After  
28 ruling out both instrumental and expansion effects, we conclude that our results provide new evidence for the  
29 importance of local kinetic processes that depend on  $\theta_{vB}$  in determining proton temperature in the solar wind.

30 1. INTRODUCTION

31 The solar wind is a variable flow of plasma that escapes  
32 from the solar corona out into the heliosphere. In-situ mea-  
33 surements of the solar wind provide insights into the funda-  
34 mental physical processes occurring in expanding astrophys-  
35 ical plasmas. Fluctuations in the solar wind plasma and elec-  
36 tromagnetic fields exist over many orders of magnitude in  
37 scale, linking both microscopic and macroscopic processes  
38 (see Matteini et al. 2012; Alexandrova et al. 2013, and refer-  
39 ences therein). The couplings between large-scale dynam-  
40 ics and small-scale kinetic processes are central to our un-  
41 derstanding of energy transport and heating in these plasmas  
42 (Verscharen et al. 2019). There are still many open questions  
43 in regards to wave dissipation and plasma heating in collision-  
44 less plasmas. Understanding these mechanisms in the colli-  
45 sionless solar wind plasma is a major outstanding problem in  
46 the field of heliophysics research.

47 In solar wind originating from open field lines in the  
48 corona, fluctuations are predominantly Alfvénic (Coleman  
49 1968; Belcher et al. 1969; Belcher & Davis Jr. 1971), with  
50 only a small compressional component (Howes et al. 2012;  
51 Klein et al. 2012; Chen 2016; Šafránková et al. 2019). At  
52 scales  $10^5 \lesssim L \lesssim 10^8$  m, called the inertial range, non-linear  
53 interactions between fluctuations lead to a turbulent cascade  
54 of energy towards smaller scales (Tu & Marsch 1995; Bruno  
55 & Carbone 2013). This range is characterised by fluctuations  
56 with increasing anisotropy toward smaller scales,  $k_{\perp} \gg k_{\parallel}$ ,

57 where  $k_{\parallel}$  and  $k_{\perp}$  are components of the wave-vector,  $\mathbf{k}$ , in the  
58 direction parallel and perpendicular to the local mean mag-  
59 netic field,  $\mathbf{B}_0$ , respectively (Horbury et al. 2008; MacBride  
60 et al. 2010; Wicks et al. 2010; Chen et al. 2011, 2012).  
61 At scales close to the proton inertial length,  $d_p$ , and pro-  
62 ton gyro-radius,  $\rho_p$ , typically  $L \sim 10^5$  m at 1 au, the prop-  
63 erties of the fluctuations change due to Hall (Galtier 2006;  
64 Galtier & Buchlin 2007) and finite-Larmor-radius (Howes  
65 et al. 2006; Schekochihin et al. 2009; Boldyrev & Perez 2012)  
66 effects. The non-linear turbulent fluctuations at these ion-  
67 kinetic scales exhibit some properties that are consistent with  
68 those of kinetic Alfvén waves (KAWs; Leamon et al. 1999;  
69 Bale et al. 2005; Howes et al. 2008; Sahraoui et al. 2010;  
70 Woodham et al. 2019).

71 Solar wind proton velocity distribution functions (VDFs)  
72 typically deviate from local thermal equilibrium due to a low  
73 rate of collisional relaxation (Kasper et al. 2008; Marsch  
74 2012; Maruca et al. 2013; Kasper et al. 2017). The cou-  
75 pling of small-scale electromagnetic fluctuations and the ki-  
76 netic features of the proton VDFs can lead to energy trans-  
77 fer between fluctuating fields and the particles. Collisionless  
78 damping of these fluctuations can lead to dissipation of turbu-  
79 lence via wave-particle interactions such as Landau (Leamon  
80 et al. 1999; Howes et al. 2008) and cyclotron (Marsch et al.  
81 1982, 2003; Isenberg & Vasquez 2019) resonance, or other  
82 processes such as stochastic heating (Chandran et al. 2010,  
83 2013) and reconnection-based mechanisms (Sundkvist et al.  
84 2007; Perri et al. 2012). These mechanisms are dependent on  
85 the modes present and the background plasma conditions, i.e.,

\*email: l.woodham@imperial.ac.uk

a function of the ratio of proton thermal pressure to magnetic pressure,  $\beta_p = n_p k_B T_p / (B_0^2 / 2\mu_0)$ , where  $n_p$  is the proton density, and  $T_p$  is the proton temperature. Each mechanism leads to distinct fine structure in proton VDFs, increasing the effective collision rate. These processes ultimately lead to plasma heating, and therefore, changes in the macroscopic properties of the plasma (e.g., Marsch 2006).

In addition to damping of turbulent fluctuations, non-Maxwellian features of solar wind VDFs such as temperature anisotropies relative to  $\mathbf{B}_0$ , beam populations, and relative drifts between plasma species provide sources of free energy for instabilities at ion-kinetic scales (Kasper et al. 2002a, 2008, 2013; Hellinger et al. 2006; Bale et al. 2009; Maruca et al. 2012; Bourouaine et al. 2013; Gary et al. 2015; Alterman et al. 2018). These modes grow until the free energy source is removed, acting to limit departure from an isotropic Maxwellian. Ion-scale kinetic instabilities are prevalent in collisionally young solar wind (Klein et al. 2018, 2019), although the interaction between instabilities and the background turbulence is still poorly understood (e.g., Klein & Howes 2015). As the solar wind flows out into the heliosphere, instabilities, local heating, heat flux, and collisions all alter the macroscopic thermodynamics of the plasma through coupling between small-scale local processes and large-scale dynamics. These processes lead to a deviation from Chew-Goldberger-Low theory (CGL; Chew et al. 1956) for double adiabatic expansion (Matteini et al. 2007).

Alfvénic fluctuations in the solar wind are characterised by magnetic field fluctuations,  $\delta\mathbf{B}$ , with a quasi-constant field magnitude,  $|\mathbf{B}|$ . Since the fluctuations have large amplitudes,  $\delta\mathbf{B}/\mathbf{B}_0 \sim 1$ , the magnetic field vector traces out a sphere of constant radius (Barnes 1981), leading to fluctuations in the angle,  $\theta_{RB}$ , between the local field,  $\mathbf{B} = \mathbf{B}_0 + \delta\mathbf{B}$ , and the radial direction. These fluctuations correlate with proton motion and therefore, the solar wind bulk velocity,  $\mathbf{v}_{sw}$ , also exhibits a dependence on  $\theta_{RB}$  (Matteini et al. 2014, 2015). If these fluctuations play a role in plasma heating, we also expect a correlation between them and the proton temperature. Recent studies have shown that the proton temperature anisotropy at 1 au exhibits a dependence on  $\theta_{RB}$  (D’Amicis et al. 2019a) that is not present closer to the Sun (Horbury et al. 2018), suggesting ongoing dynamical processes related to these fluctuations in the solar wind. In fact, larger wave power in transverse Alfvénic fluctuations is also correlated with proton temperature anisotropy (Bourouaine et al. 2010), consistent with an increase in fluctuations in  $\theta_{RB}$ .

Single-spacecraft observations have an inherent spatio-temporal ambiguity that complicates investigation of the coupling between Alfvénic fluctuations and the plasma bulk parameters. These measurements are restricted to the sampling of a time series defined by the trajectory of the spacecraft with respect to the flow velocity,  $\mathbf{v}_{sw}$ . This limitation means that we can only resolve the component of  $\mathbf{k}$  along the sampling direction, i.e., predominantly the radial direction. Previous studies (e.g., Horbury et al. 2008; Wicks et al. 2010; He et al. 2011; Podesta & Gary 2011b) assume that the underlying distribution of turbulence in the solar wind is independent of  $\theta_{vB}$ , the angle between  $\mathbf{v}_{sw}$  and  $\mathbf{B}_0$ . Based on this assumption, these studies use measurements of the solar wind plasma at different  $\theta_{vB}$  to probe the turbulence as a function of  $\theta_{kB}$ , the angle between  $\mathbf{k}$  and  $\mathbf{B}_0$ . However, if there is indeed a dependence of the plasma bulk parameters (including the temperature and temperature anisotropies as observed) on  $\theta_{RB} \simeq \theta_{vB}$ , then this

assumption may not be valid.

In this paper, we investigate whether the solar wind proton temperature anisotropy depends on the polarisation properties of small-scale Alfvénic fluctuations, and hence  $\theta_{vB}$ , in the context of turbulent dissipation. In Section 2, we discuss the linear theory and polarisation properties of Alfvén waves. In Sections 3 and 4, we describe our analysis methods, using single-spacecraft measurements to measure the polarisation properties of Alfvénic fluctuations at ion-kinetic scales in the solar wind. We present our main results in Section 5, testing how the dissipation of turbulence at these scales affects the macroscopic bulk properties of the solar wind. We show that Alfvénic fluctuations present at ion-kinetic scales in the solar wind share at least some polarisation properties with Alfvén waves from linear Vlasov theory. By also investigating the statistical distribution of proton temperature in the  $\beta_p$ - $\theta_{vB}$  plane, we find that there is a clear dependence in this reduced parameter space that also correlates with the magnetic helicity of Alfvénic fluctuations. We discuss the implications of our results in Section 6, namely that we cannot sample different  $\theta_{vB}$  to analyse the dependence of the turbulence on  $\theta_{kB}$  without considering other plasma properties. In Section 7, we consider both instrumental and expansion effects, showing that they do not account for the observed temperature distribution. Finally, in Section 8, we conclude that our results provide new evidence for the importance of local kinetic processes that depend on  $\theta_{vB}$  in determining proton temperature in the solar wind.

## 2. POLARISATION PROPERTIES OF ALFVÉN WAVES

In collisionless space plasmas such as the solar wind, the linearised Vlasov equation describes linear waves and instabilities. Non-trivial solutions exist only when the complex frequency,  $\omega = \omega_r + i\gamma$ , solves the hot-plasma dispersion relation (Stix 1992). Here,  $\omega_r$  is the wave frequency and  $\gamma$  is the wave growth ( $\gamma > 0$ ) or damping ( $\gamma < 0$ ) rate. One such solution is the Alfvén wave, which is ubiquitous in space plasmas. At  $k_{\parallel} d_p \ll 1$  and  $k_{\perp} \rho_p \ll 1$ , this wave is incompressible and propagates along  $\mathbf{B}_0$  at the Alfvén speed,  $v_A$ , resulting in transverse perturbations to the field (Alfvén 1942). The fluctuations in velocity,  $\delta\mathbf{v}$ , and the magnetic field,  $\delta\mathbf{b}$ , exhibit a characteristic (anti-)correlation,  $\delta\mathbf{v} = \mp\delta\mathbf{b}$ , for propagation (parallel) anti-parallel to  $\mathbf{B}_0$ . Here,  $\mathbf{b}$  is the magnetic field in Alfvén units,  $\mathbf{b} = \mathbf{B}/\sqrt{\mu_0\rho}$ , where  $\rho$  is the plasma mass density. The Alfvén wave has the dispersion relation:

$$\omega_r(k) = kv_A \cos\theta_{kB}. \quad (1)$$

Approaching ion-kinetic scales,  $k_{\parallel} d_p \simeq 1$  or  $k_{\perp} \rho_p \simeq 1$ , the dispersion relation splits into two branches: the Alfvén ion-cyclotron (AIC) wave for small  $\theta_{kB}$  (Gary & Borovsky 2004) and the KAW for large  $\theta_{kB}$  (Gary & Nishimura 2004).

We define the polarisation of a wave as:

$$P = -\frac{i\delta E_y}{\delta E_x} \frac{\omega_r}{|\omega_r|}, \quad (2)$$

where  $\delta E_x$  and  $\delta E_y$  are components of the Fourier amplitudes of the fluctuating electric field transverse to  $\mathbf{B}_0 = B_0 \hat{\mathbf{z}}$  (Stix 1992; Gary 1993). Therefore,  $P$  gives the sense and degree of rotation in time of a fluctuating electric field vector at a fixed point in space, viewed in the direction parallel to  $\mathbf{B}_0$ . A circularly polarised wave has  $P = \pm 1$ , where +1 (-1) designates right-handed (left-handed) polarisation. In this definition, a

205 right-hand polarised wave has electric field vectors that rotate  
 206 in the same sense as the gyration of an electron, and a  
 207 left-hand polarised wave, the same sense as ions. For more  
 208 general elliptical polarisation, we take the real part,  $\text{Re}(P)$ .

209 Magnetic helicity is a measure of the degree and sense of  
 210 spatial rotation of the magnetic field (Woltjer 1958a,b). It is  
 211 an invariant of ideal magnetohydrodynamics (MHD) and defined  
 212 as a volume integral over all space:

$$H_m \equiv \int_V \mathbf{A} \cdot \mathbf{B} d^3\mathbf{r}, \quad (3)$$

213 where  $\mathbf{A}$  is the magnetic vector potential defined by  $\mathbf{B} =$   
 214  $\nabla \times \mathbf{A}$ . Matthaeus et al. (1982) propose the fluctuating mag-  
 215 netic helicity,  $H'_m(\mathbf{k})$ , as a diagnostic of solar wind fluctua-  
 216 tions, which in spectral form (i.e., in Fourier space) is defined  
 217 as:

$$H'_m(\mathbf{k}) \equiv \delta\mathbf{A}(\mathbf{k}) \cdot \delta\mathbf{B}^*(\mathbf{k}), \quad (4)$$

218 where  $\delta\mathbf{A}$  is the fluctuating vector potential, and the aster-  
 219 isk indicates the complex conjugate of the Fourier coefficients  
 220 (Matthaeus & Goldstein 1982b). This definition removes con-  
 221 tributions to the helicity arising from  $\mathbf{B}_0$ . By assuming the  
 222 Coulomb gauge,  $\nabla \cdot \mathbf{A} = 0$ , the fluctuating magnetic helicity  
 223 can be written:

$$H'_m(\mathbf{k}) = i \frac{\delta B_y \delta B_z^* - \delta B_y^* \delta B_z}{k_x}, \quad (5)$$

224 where the components of  $\delta\mathbf{B}(\mathbf{k})$  are Fourier coefficients of a  
 225 wave mode with  $\mathbf{k}$ . This result is invariant under cyclic per-  
 226 mutations of the three components  $x, y, z$  (See Equation 2 in  
 227 Howes & Quataert 2010). We define the normalised fluctuat-  
 228 ing magnetic helicity density as:

$$\sigma_m(\mathbf{k}) \equiv \frac{k H'_m(\mathbf{k})}{|\delta\mathbf{B}(\mathbf{k})|^2}, \quad (6)$$

229 where  $|\delta\mathbf{B}(\mathbf{k})|^2 = \delta B_x^* \delta B_x + \delta B_y^* \delta B_y + \delta B_z^* \delta B_z$ . Here,  $\sigma_m(\mathbf{k})$  is  
 230 dimensionless and takes values in the interval  $[-1, 1]$ , where  
 231  $\sigma_m = -1$  indicates fluctuations with purely left-handed helicity,  
 232 and  $\sigma_m = +1$  purely right-handed helicity. A value of  $\sigma_m = 0$   
 233 indicates no overall coherence, i.e., there are either no fluctua-  
 234 tions with coherent handedness or there is equal power in  
 235 both left-handed and right-handed components so that the net  
 236 value is zero.

237 Gary (1986) first explored the dependence of  $\text{Re}(P)$  for  
 238 small-scale Alfvén waves on different parameters by numeri-  
 239 cally solving the full electromagnetic dispersion relation,  
 240 showing that it changes sign depending on both  $\theta_{kB}$  and  
 241  $\beta_p$ . In the cold-plasma limit ( $\beta_p \ll 1$ ), the Alfvén wave has  
 242  $\text{Re}(P) < 0$  for all  $\theta_{kB}$ . However, from linear Vlasov theory, at  
 243  $\beta_p \simeq 10^{-2}$ , the wave has  $\text{Re}(P) < 0$  for  $0^\circ \leq \theta_{kB} \lesssim 80^\circ$ , but  
 244 has  $\text{Re}(P) > 0$  for  $\theta_{kB} \gtrsim 80^\circ$ . As  $\beta_p$  increases, the wave has  
 245  $\text{Re}(P) > 0$  for an increasing range of oblique angles so that at  
 246  $\beta_p \simeq 10$ , the transition occurs at about  $40^\circ$ . This result reveals  
 247 that the changing polarisation properties on both  $\theta_{kB}$  and  $\beta_p$   
 248 will affect possible wave-particle interactions, and hence tur-  
 249 bulence damping mechanisms that can occur in a plasma. For  
 250 example, left-handed AIC waves can cyclotron resonate with  
 251 ions, leading to heating perpendicular to  $\mathbf{B}_0$ . On the other  
 252 hand, right-handed KAWs are compressive at small scales,  
 253 giving rise to density fluctuations and a non-zero component

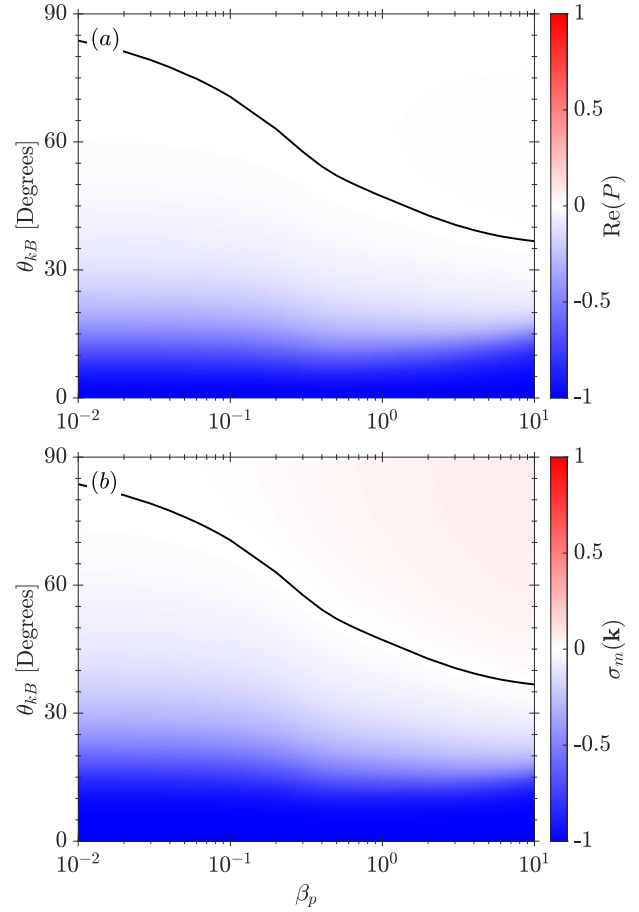


**Figure 1.** (a) The real part of the polarisation,  $\text{Re}(P)$ , and (b) normalised fluctuating magnetic helicity density,  $\sigma_m(\mathbf{k})$ , of Alfvén waves with  $kd_p = 0.05$  as a function of  $\beta_p$  and  $\theta_{kB}$ , calculated using the NHDS code (see main text). The black lines indicate the isocontours  $\text{Re}(P) = 0$  and  $\sigma_m(\mathbf{k}) = 0$ .

of the wave electric field,  $E_{\parallel} \neq 0$ . Hence, KAWs can Landau resonate with both electrons and ions, leading to heating parallel to  $\mathbf{B}_0$ .

We plot both  $\text{Re}(P)$  and  $\sigma_m(\mathbf{k})$  for Alfvénic fluctuations across the  $\beta_p$ - $\theta_{kB}$  plane in Figure 1. The black lines are isocontours of  $\text{Re}(P) = 0$  and  $\sigma_m(\mathbf{k}) = 0$ , respectively. We note that for waves with  $\theta_{kB} \simeq 0$ , there is no difference between the values of  $\text{Re}(P)$  and  $\sigma_m(\mathbf{k})$ . To calculate these lines, we solve the linear Vlasov equation using the New Hampshire Dispersion relation Solver (NHDS; Verscharen et al. 2013; Verscharen & Chandran 2018). Here,  $\mathbf{k} = k_{\perp} \hat{\mathbf{x}} + k_{\parallel} \hat{\mathbf{z}}$ , and we assume a plasma consisting of protons and electrons with isotropic Maxwellian distributions, equal density and temperature, and no drifting components. We set  $kd_p = 0.05$ ,<sup>1</sup> where the angle  $\theta_{kB}$  defines  $k_{\perp} = k \sin \theta_{kB}$  and  $k_{\parallel} = k \cos \theta_{kB}$ . Therefore,  $k_{\parallel} d_p$  and  $k_{\perp} \rho_p$  change throughout the  $\beta_p$ - $\theta_{kB}$  plane,<sup>2</sup> while the normalised scale of the waves remains constant. We also set  $v_A/c = 10^{-4}$ , which is typical for solar wind conditions where  $v_A \simeq 50$  km/s (Klein et al. 2019). While our assumption of an isotropic proton-electron plasma is not truly representative of the more complex ion VDFs typically observed in the solar wind, protons remain the most important ion component for solar wind interaction with Alfvénic fluctuations. Therefore, we expect that the polarisation properties of Alfvénic

<sup>1</sup> The black lines in Figure 1 are constant over the range:  $kd_p = [0.01, 1]$ .

<sup>2</sup> The scales  $d_p$  and  $\rho_p$  are related by:  $\rho_p = d_p \sqrt{\beta_p}$ .

fluctuations in the solar wind are adequately described by the theoretical description provided in Figure 1.

### 3. REDUCED SPECTRA FROM SPACECRAFT MEASUREMENTS

In the solar wind, the polarisation properties of fluctuations are typically determined using the fluctuating magnetic helicity. However, from a single-spacecraft time series of magnetic field measurements, it is only possible to determine a reduced form of the helicity (Batchelor 1970; Montgomery & Turner 1981; Matthaeus et al. 1982):

$$H_m^{rr}(\omega_{sc}) = \frac{2 \text{Im} \{ \mathcal{P}_{TN}^r(\omega_{sc}) \}}{k_r}, \quad (7)$$

where  $\omega_{sc}$  is the frequency of the fluctuations in the spacecraft frame,  $k_r = k \cos \theta_{kv}$  is the component of the wave-vector along the flow direction of the solar wind plasma,  $\mathbf{v}_{sw}$ , and  $\theta_{kv}$  is the angle between  $\mathbf{k}$  and  $\mathbf{v}_{sw}$ . Here,

$$\mathcal{P}_{ij}^r(\omega_{sc}) = \delta B_i^*(\omega_{sc}) \cdot \delta B_j(\omega_{sc}) \quad (8)$$

is the reduced power spectral tensor, where the  $\delta B_i(\omega_{sc})$  are the complex Fourier coefficients of the time series of  $\mathbf{B}$  in radial-tangential-normal (RTN) coordinates.<sup>3</sup> In this coordinate system, the solar wind flow is approximately radial,  $\mathbf{v}_{sw} \simeq v_{sw} \hat{\mathbf{R}}$ . The reduced tensor is an integral of the true spectral tensor,  $\mathcal{P}_{ij}(\mathbf{k})$  (Fredricks & Coroniti 1976; Forman et al. 2011; Wicks et al. 2012):

$$\mathcal{P}_{ij}^r(\omega_{sc}) = \int \mathcal{P}_{ij}(\mathbf{k}) \delta [\omega_{sc} - (\mathbf{k} \cdot \mathbf{v}_{sw} + \omega_{pl})] d^3 \mathbf{k}. \quad (9)$$

Taylor's hypothesis (Taylor 1938) assumes that the fluctuations in the solar wind evolve slowly as they are advected past the spacecraft so that the plasma-frame frequency,  $\omega_{pl}$ , satisfies  $|\omega_{pl}| \ll |\mathbf{k} \cdot \mathbf{v}_{sw}|$  (Matthaeus & Goldstein 1982b; Perri & Balogh 2010). Therefore, the Doppler shift of the fluctuations into the spacecraft frame becomes:

$$\omega_{sc} = \omega_{pl} + \mathbf{k} \cdot \mathbf{v}_{sw} \simeq \mathbf{k} \cdot \mathbf{v}_{sw} \equiv k_r v_{sw}, \quad (10)$$

so that the  $\omega_{pl}$  term drops from Equation 9. Then, a time series of magnetic field measurements under these assumptions represents a spatial cut through the plasma and we can write  $\mathcal{P}_{ij}^r$  and  $H_m^{rr}$  as functions  $k_r$  using Equation 10. However, it is not possible to determine the full wave-vector,  $\mathbf{k}$ , or  $\theta_{kB}$ , from single-spacecraft measurements. Since  $v_A \ll v_{sw}$ , Taylor's hypothesis is usually well-satisfied for Alfvén waves in the solar wind with the dispersion relation given by Equation 1, as well as for the small-wavelength extensions of the Alfvén branch under the parameters considered here (see Howes et al. 2014; Klein et al. 2014a).

Based on the definition in Equation 6, the normalised reduced fluctuating magnetic helicity density is then defined as:

$$\sigma_m^r(k_r) \equiv \frac{k_r H_m^{rr}(k_r)}{|\delta \mathbf{B}(k_r)|^2} = \frac{2 \text{Im} \{ \mathcal{P}_{TN}^r(k_r) \}}{\text{Tr} \{ \mathcal{P}^r(k_r) \}}, \quad (11)$$

where  $\text{Tr}\{\}$  denotes the trace. Previous studies (e.g., Horbury et al. 2008; Wicks et al. 2010; He et al. 2011; Podesta & Gary 2011b) use  $\theta_{vB}$  as a measure of a specific  $\theta_{kB}$  in

the solar wind. For example, measurements of  $\sigma_m^r(k_r)$  separated as a function of  $\theta_{vB}$  show a broad right-handed signature at oblique angles and a narrow left-handed signature at quasi-parallel angles (He et al. 2011, 2012a,b; Podesta & Gary 2011b; Klein et al. 2014b; Bruno & Telloni 2015; Telloni et al. 2015). These signatures are associated with KAW-like fluctuations from the turbulent cascade and ion-kinetic instabilities, respectively (Telloni & Bruno 2016; Woodham et al. 2019).

By defining the field-aligned coordinate system,

$$\hat{\mathbf{z}} = \frac{\mathbf{B}_0}{|\mathbf{B}_0|}; \hat{\mathbf{y}} = -\frac{\mathbf{v}_{sw} \times \mathbf{B}_0}{|\mathbf{v}_{sw} \times \mathbf{B}_0|}; \hat{\mathbf{x}} = \hat{\mathbf{y}} \times \hat{\mathbf{z}}, \quad (12)$$

so that  $\mathbf{v}_{sw}$  lies in the  $x$ - $z$  plane with angle  $\theta_{vB}$  from the  $\hat{\mathbf{z}}$  direction (Wicks et al. 2012; Woodham et al. 2019), we can decompose  $\sigma_m^r(k_r)$  into the components:

$$\sigma_{ij}(k_l) = \frac{2 \text{Im} \{ \mathcal{P}_{ij}^r(k_l) \}}{\text{Tr} \{ \mathcal{P}^r(k_l) \}}, \quad (13)$$

where the indices  $i, j, l = x, y, z$ . We derive the following relationship between the components,  $\sigma_{ij}(k_l)$ , and  $\sigma_m^r(k_r)$  (see Appendix):

$$\sigma_{xy}(k_z) = \sigma_m^r(k_r) \frac{k_z}{k_r}, \quad (14)$$

$$\sigma_{xz}(k_y) = -\sigma_m^r(k_r) \frac{k_y}{k_r}, \quad (15)$$

and

$$\sigma_{yz}(k_x) = \sigma_m^r(k_r) \frac{k_x}{k_r}. \quad (16)$$

For fluctuations with  $k_z \gg k_x$ , i.e.,  $\mathbf{k}$  quasi-parallel to  $\mathbf{B}_0$ ,  $\sigma_{xy}(k_z)$  is the dominant contribution to  $\sigma_m^r(k_r)$ . Similarly,  $\sigma_{yz}(k_x)$  dominates for modes with  $k_x \gg k_z$ , i.e.,  $\mathbf{k}$  at oblique angles,  $\theta_{kB} \gtrsim 60^\circ$ . As the solar wind velocity is confined to the  $x$ - $z$  plane, we have no information about  $k_y$  from single-spacecraft measurements and  $\sigma_{xz}(k_y)$  is not useful in a practical sense. From Section 2, we expect that AIC waves generated by kinetic instabilities have  $k_z \gg k_x$ . The anisotropic Alfvénic turbulent cascade leads to the generation of nearly perpendicular wave-vectors with  $k_x \gg k_z$ . Therefore, we can separate the helicity signatures of the two kinetic scale branches of the Alfvén wave using our decomposition technique.

## 4. DATA ANALYSIS

We analyse magnetic field data from the MFI fluxgate magnetometer (Lepping et al. 1995; Koval & Szabo 2013) and proton data from the SWE Faraday cup (Ogilvie et al. 1995; Kasper et al. 2006) instruments on-board the *Wind* spacecraft from Jun 2004 to Oct 2018. For each proton measurement, we define a local mean field,  $\mathbf{B}_0$ , averaged over the SWE integration time ( $\sim 92$  s). We estimate the normalised cross-helicity (Matthaeus & Goldstein 1982a) for each  $\sim 92$  s interval,

$$\sigma_c = \frac{2(\delta \mathbf{v} \cdot \delta \mathbf{b})}{|\delta \mathbf{v}|^2 + |\delta \mathbf{b}|^2}, \quad (17)$$

where  $\delta \mathbf{b} = \mathbf{b} - \langle \mathbf{b} \rangle_{1h}$  and  $\delta \mathbf{v} = \mathbf{v}_{sw} - \langle \mathbf{v}_{sw} \rangle_{1h}$ . Here, the mean is over a one hour window centred on the instantaneous values and we assume that  $\mathbf{v}_{sw} \simeq \mathbf{v}_p$ , where  $\mathbf{v}_p$  is the proton bulk

<sup>3</sup> In the RTN coordinate system,  $\hat{\mathbf{R}}$  is the unit vector from the Sun towards the spacecraft,  $\hat{\mathbf{T}}$  is the cross-product of the solar rotation axis and  $\hat{\mathbf{R}}$ , and  $\hat{\mathbf{N}}$  completes the right-handed triad.

361 velocity. An averaging interval of one hour gives  $\sigma_c$  for fluctu-  
 362 ations in the inertial range. The cross-helicity,  $\sigma_c \in [-1, 1]$ ,  
 363 is a measure of the (anti-)correlation between velocity and  
 364 magnetic field fluctuations, and therefore, Alfvénicity (e.g.,  
 365 D’Amicis & Bruno 2015; D’Amicis et al. 2019b; Stansby  
 366 et al. 2019; Perrone et al. 2020). A value  $|\sigma_c| = 1$  indicates  
 367 purely unbalanced Alfvénic fluctuations propagating in one  
 368 direction, whereas  $\sigma_c = 0$  indicates either balanced (equal  
 369 power in opposite directions) or a lack of Alfvénic fluctu-  
 370 ations. In case of  $\sigma_c = 0$ , we expect no coherent value of  
 371  $|\sigma_m| > 0$  at ion-kinetic scales.

372 Similarly to Woodham et al. (2019), we account for helio-  
 373 spheric sector structure in the magnetic field measurements  
 374 by calculating  $\sigma_c$  averaged over a running window of 12  
 375 hours. For solar wind fluctuations dominantly propagating  
 376 anti-sunward, the sign of  $\sigma_c$  depends only on the direction of  
 377  $\mathbf{B}_0$ . Therefore, if  $\langle \sigma_c \rangle > 0$ , we reverse the signs of the  $B_R$   
 378 and  $B_T$  components for each  $\sim 92$  s measurement so that sun-  
 379 ward fields are rotated anti-sunward. This procedure removes  
 380 the inversion of the sign of magnetic helicity due to the di-  
 381 rection of the large-scale magnetic field with respect to the  
 382 Sun.<sup>4</sup> We transform the 11 Hz magnetic field data associated  
 383 with each proton measurement into field-aligned coordinates  
 384 (Equation 12) using  $\mathbf{B}_0$  averaged over  $\sim 92$  s. We then com-  
 385 pute the continuous wavelet transform (Torrence & Compo  
 386 1998) using a Morlet wavelet to calculate the magnetic heli-  
 387 city spectra,  $\sigma_{xy}$  and  $\sigma_{yz}$ , as functions of  $f_{sc} = \omega_{sc}/2\pi$  using  
 388 Equation 13. We average the spectra over  $\sim 92$  s, correspond-  
 389 ing to the SWE measurement cadence, to ensure that the fluctu-  
 390 ations contributing to the helicity spectra persist for at least  
 391 several proton gyro-periods,  $2\pi/\Omega_p$ , giving a clear coherent  
 392 helicity signature at ion-kinetic scales.

393 We estimate the amplitudes of  $\sigma_{xy}$  and  $\sigma_{yz}$  at ion-kinetic  
 394 scales by fitting a Gaussian function to the coherent peak  
 395 in each spectrum at frequencies close to the Taylor-shifted  
 396 frequencies,  $v_{sw}/d_p$  and  $v_{sw}/\rho_p$  (see Woodham et al. 2018).  
 397 We neglect any peak at  $f > f_{noise}$ , where  $f_{noise}$  is the fre-  
 398 quency above which instrumental noise of the MFI magne-  
 399 tometer becomes significant.<sup>5</sup> We also reject a spectrum if  
 400 the angular deviation in  $\mathbf{B}$  exceeds  $15^\circ$  during the  $\sim 92$  s mea-  
 401 surement period to ensure that we measure the anisotropy of  
 402 fluctuations at ion-kinetic scales with sufficient accuracy (see  
 403 also Section 7.1). We designate the amplitude of the peak  
 404 in each  $\sigma_{xy}$  spectrum as  $\sigma_{\parallel} \equiv \max_{k_z} \sigma_{xy}(k_z)$  to diagnose the  
 405 helicity of the modes with  $\mathbf{k}$  quasi-parallel to  $\mathbf{B}_0$ , and  $\sigma_{\perp}$  as  
 406  $\sigma_{\perp} \equiv \max_{k_x} \sigma_{yz}(k_x)$  to diagnose the helicity of the modes with  
 407  $\mathbf{k}$  oblique to  $\mathbf{B}_0$  (see Section 3 and Appendix).

408 In our analysis, we include only measurements of Alfvénic  
 409 solar wind,  $|\sigma_c| \geq 0.8$ , and low collisionality,  $N_c < 1$ , which  
 410 contain the strongest Alfvénic fluctuations with a non-zero  
 411 magnetic helicity. Here,  $N_c$  is the Coulomb number (Maruca  
 412 et al. 2013; Kasper et al. 2017), which estimates the number  
 413 of collisional timescales for protons. We calculate  $N_c$  using  
 414 the proton-proton collision frequency, neglecting collisions  
 415 between protons and other ions. We bin the data in  $\log_{10}(\beta_p)$   
 416 and  $\theta_{vB}$  using bins of width  $\Delta \log_{10}(\beta_p) = 0.05$  and  $\Delta \theta_{vB} = 5^\circ$ .  
 417 We restrict our analysis to  $0.01 \leq \beta_p \leq 10$  and include the full  
 418 range of  $\theta_{vB} = [0^\circ, 180^\circ]$  to account for any dependence on he-  
 419 liospheric sector structure. In Figure 2, we plot the probability  
 420 density distribution of the data,

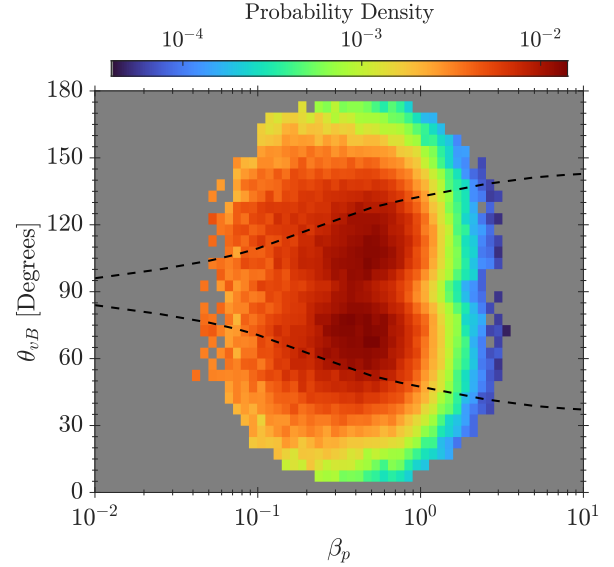


**Figure 2.** Probability density distribution of solar wind data in the  $\beta_p$ - $\theta_{vB}$  plane, calculated using Equation 18. The dashed black lines indicate the isocontours of  $\tilde{\sigma}_m(\theta_{vB}) = 0$  mirrored about the line  $\theta_{vB} = 90^\circ$  (see main text).

$$\tilde{p} = \frac{n}{N \Delta \beta_p \Delta \theta_{vB}}, \quad (18)$$

421 in the  $\beta_p$ - $\theta_{vB}$  plane, where  $n$  is the number of data points in  
 422 each bin and  $N$  is the total number of data points. We over-  
 423 plot the isocontour of  $\sigma_m(\mathbf{k}) = 0$  from Figure 1(b) by replacing  
 424  $\theta_{kB}$  with  $\theta_{vB}$ , i.e.,  $\tilde{\sigma}_m(\theta_{vB}) = 0$ . If we assume the turbulence  
 425 is independent of  $\theta_{vB}$ , then any dependence on  $\theta_{vB}$  exclusively  
 426 reflects a dependence on  $\theta_{kB}$  (see Horbury et al. 2008; Wicks  
 427 et al. 2010; He et al. 2011; Podesta & Gary 2011b). We mirror  
 428 the  $\tilde{\sigma}_m(\theta_{vB}) = 0$  curve around the line  $\theta_{vB} = 90^\circ$  to account for  
 429 heliospheric sector structure. The distribution of data in Fig-  
 430 ure 2 shows two peaks at  $\theta_{vB} \sim 70^\circ$  and  $\theta_{vB} \sim 110^\circ$  around  
 431  $\beta_p \sim 0.5$ . There are fewer data points at quasi-parallel an-  
 432 gles, showing that the majority of data are associated with  
 433 oblique angles. Naïvely, one would expect the distribution to  
 434 follow the large-scale Parker spiral, peaking at angles  $\sim 45^\circ$   
 435 and  $\sim 135^\circ$ . However, we note that  $\theta_{vB}$  is calculated at  $\sim 92$   
 436 s timescales, over with the local mean field  $\mathbf{B}_0$  has already  
 437 been deflected from the Parker spiral by Alfvénic fluctuations  
 438 present at larger scales. There is also a clear  $\beta_p$  dependence  
 439 in Figure 2, with the majority of the data lying in the range  
 440  $0.1 \lesssim \beta_p \lesssim 1$ , which is typical for quiescent solar wind (Wil-  
 441 son III et al. 2018).

## 5. RESULTS

442 In Figure 3, we plot the median values of  $\sigma_{\parallel}$  and  $\sigma_{\perp}$  for  
 443 each bin in the  $\beta_p$ - $\theta_{vB}$  plane. We neglect any bins with fewer  
 444 than 20 data points to improve statistical reliability. From  
 445 Figure 1, we expect to measure KAW-like fluctuations with  
 446  $\sigma_{\perp} > 0$  in the area of the  $\beta_p$ - $\theta_{vB}$  plane enclosed by the two  
 447 dashed lines at quasi-perpendicular angles, and AIC wave-  
 448 like fluctuations with  $\sigma_{\parallel} < 0$  at quasi-parallel angles. Figure  
 449 3 is consistent with this expectation; we see a strong negative  
 450 helicity signal at  $0^\circ \leq \theta_{vB} \leq 30^\circ$  and  $150^\circ \leq \theta_{vB} \leq 180^\circ$ , with  
 451 a minimum of  $\sigma_{\parallel} \simeq -0.8$  approaching  $\theta_{vB} \simeq 0^\circ$ , as well as  
 452 a weaker positive signal of  $\sigma_{\perp} \simeq 0.4$  at angles  $60^\circ \leq \theta_{vB} \leq$   
 453  $120^\circ$ . Both  $\sigma_{\parallel}$  and  $\sigma_{\perp}$  are symmetrically distributed about  
 454 the line  $\theta_{vB} = 90^\circ$  since we remove the ambiguity in the sign  
 455

<sup>4</sup> See Table 1 in Woodham et al. (2019).

<sup>5</sup> See Appendix in Woodham et al. (2018).

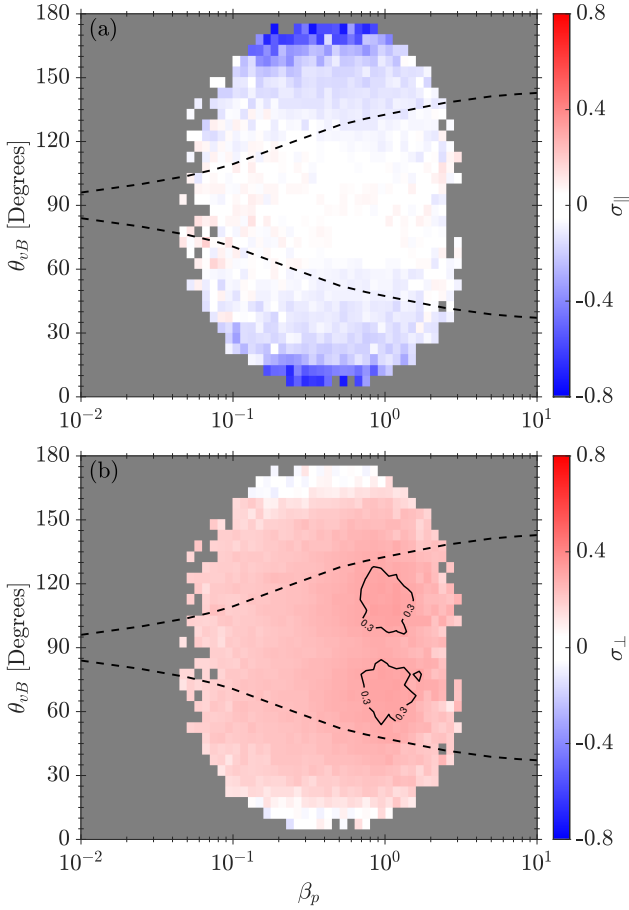


**Figure 3.** (a) Median  $\sigma_{\parallel}$  and (b) median  $\sigma_{\perp}$  across the  $\beta_p$ - $\theta_{vB}$  plane. The dashed black lines indicate the isocontours of  $\sigma_{\parallel}(\theta_{vB}) = 0$  mirrored about the line  $\theta_{vB} = 90^\circ$ . We also include contours of constant  $\sigma_{\perp} = 0.3$  in Panel (b) as solid black lines.

of the helicity due to the direction of  $\mathbf{B}_0$ . The distribution of  $\sigma_{\parallel}$  is consistent with the presence of quasi-parallel propagating AIC waves from kinetic instabilities in the solar wind (Woodham et al. 2019; Zhao et al. 2018, 2019a). Elsewhere in Figure 3(a), the median value of  $\sigma_{\parallel}$  is zero, showing that a coherent signal of parallel-propagating fluctuations at ion-kinetic scales in the solar wind is not measured at oblique angles.

In Figure 3(b), there are two peaks in the median  $\sigma_{\perp}$  close to  $\beta_p \sim 1$ , located at  $\theta_{vB} \sim 70^\circ$  and  $\theta_{vB} \sim 110^\circ$ . Despite these peaks, the signal is spread across the parameter space, except at quasi-parallel angles where  $\sigma_{\perp} \simeq 0$ . We interpret this spread using Taylor’s hypothesis. Due to the  $\mathbf{k} \cdot \mathbf{v}_{sw}$  term in the  $\delta$ -function in Equation 9, a  $\cos \theta_{kv}$  factor modifies the contribution of all modes to the reduced spectrum measured in the direction of  $\mathbf{v}_{sw}$ . If  $\theta_{kv} = 0^\circ$ , then  $\cos \theta_{kv} = 1$ , and the waves are measured at their actual  $k$ . However, oblique modes measured at a fixed  $\omega_{sc}$  correspond to a higher  $k$  in the plasma frame. Since the turbulent spectrum decreases in amplitude with increasing  $k$ , the reduced spectrum is most sensitive to the smallest  $\mathbf{k}$  in the sampling direction. For parallel propagating fluctuations such as AIC waves,  $\theta_{vB} \simeq \theta_{kv}$ , but for a broader  $k$ -distribution of obliquely propagating fluctuations, multiple fluctuations with different  $\mathbf{k}$  and therefore, different  $\theta_{kB}$ , contribute to a single  $\theta_{vB}$  bin. The signal at  $\theta_{vB} \lesssim 30^\circ$  is then likely due to fluctuations with  $\theta_{kB} \gtrsim 60^\circ$ , since they contribute to  $\sigma_{\perp}$ , i.e., have a significant  $k_{\perp}$  component.

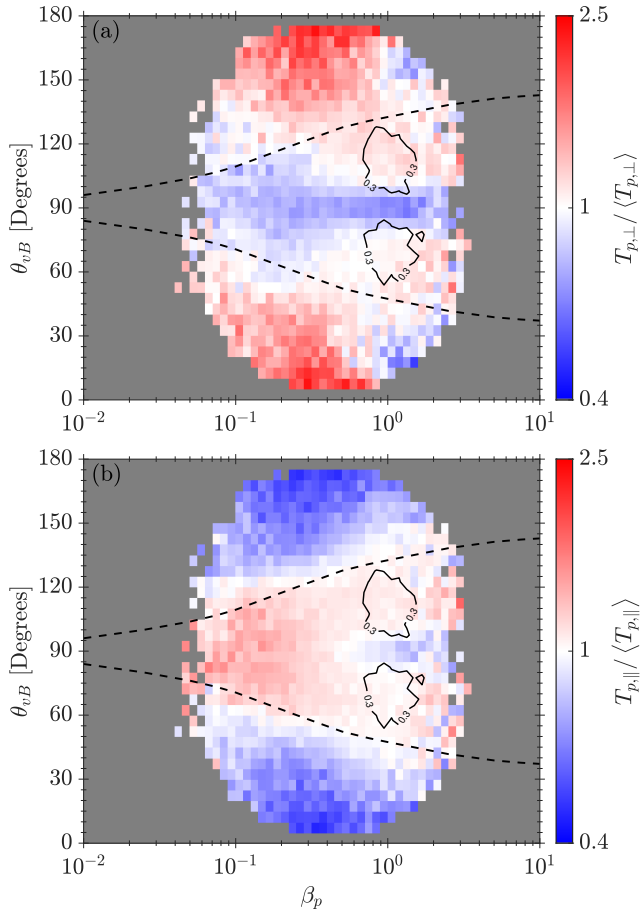
As the polarisation properties of small-scale Alfvénic fluctuations are consistent with predictions from linear theory, it is reasonable to expect that  $T_p$  is also correlated in the  $\beta_p$ - $\theta_{vB}$  plane. This expectation follows because different Alfvénic fluctuations are associated with different dissipation mechanisms, leading to distinct heating signatures. On the other hand, if the properties of the turbulence are truly independent of  $\theta_{vB}$ , then we expect the dissipation mechanisms, and therefore, proton heating to be independent of  $\theta_{vB}$ . To test this hypothesis, we plot the median values of  $T_{p,\perp}/\langle T_{p,\perp} \rangle$  and  $T_{p,\parallel}/\langle T_{p,\parallel} \rangle$  for each bin in the  $\beta_p$ - $\theta_{vB}$  plane in Figure 4. Here,  $\langle T_{p,\perp/\parallel} \rangle$  is the average value of  $T_{p,\perp/\parallel}$  over all angles for each bin in  $\log_{10}(\beta_p)$ . This column normalisation removes the systematic proportionality of  $T_p$  with  $\beta_p$ . The colour of each bin in the  $\theta_{vB}$ - $\beta_p$  plane, therefore, shows as a function of  $\theta_{vB}$  whether the proton temperature is equal to, larger than, or smaller than the average for a specific  $\beta_p$ .

Figure 4 shows a clear dependence of the median column-normalised  $T_{p,\perp}$  and  $T_{p,\parallel}$  on both  $\theta_{vB}$  and  $\beta_p$ . In general, we see higher  $T_{p,\perp}/\langle T_{p,\perp} \rangle$  at quasi-parallel angles where  $\sigma_{\parallel}$  is largest in Figure 3(a), associated with AIC waves driven by kinetic instabilities (Kasper et al. 2002b; Matteini et al. 2007; Bale et al. 2009; Maruca et al. 2012; Woodham et al. 2019). We also see higher  $T_{p,\parallel}/\langle T_{p,\parallel} \rangle$  at oblique angles where  $\sigma_{\perp}$  is largest in Figure 3(b), associated with KAW-like fluctuations (Leamon et al. 1999; Bale et al. 2005; Howes et al. 2008; Sahraoui et al. 2010). However, there are also enhancements in  $T_{p,\perp}/\langle T_{p,\perp} \rangle$  where  $\sigma_{\perp} \simeq 0.3$ , as indicated by the contours of constant  $\sigma_{\perp}$  from Figure 3(b). Despite enhancements in both the column-normalised  $T_{p,\perp}$  and  $T_{p,\parallel}$  in this region of parameter space, the proton temperature remains anisotropic with  $T_{p,\perp}/T_{p,\parallel} < 1$ . We note that a lack of helicity signature does not imply that waves are not present. Therefore, if the enhancements in proton temperature are associated with different dissipation mechanisms, we do not expect a perfect correlation with  $\sigma_{\parallel}$  and  $\sigma_{\perp}$  in the  $\theta_{vB}$ - $\beta_p$  plane.

Hellinger & Trávníček (2014) recommend to exercise caution when bin-averaging solar wind data in a reduced parameter space. While conditional statistics have been employed in several studies (e.g., Bale et al. 2009; Maruca et al. 2011; Osman et al. 2012), this non-trivial procedure may give spurious results as a consequence of superposition of multiple correlations in the solar wind and should be interpreted cautiously. We find no evidence that the correlations shown in Figure 4 are caused by or related to other underlying correlations in the solar wind multi-dimensional parameter space. In particular, we rule out the known correlation between  $v_{sw}$  and  $T_p$  (Matthaeus et al. 2006; Perrone et al. 2019) by separating our results as a function of solar wind speed, finding that Figure 4 is largely unchanged (not shown). This is consistent with the fact that the  $\beta_p$ - $\theta_{vB}$  parameter space we investigate is determined by the properties of Alfvénic fluctuations, which exist in both fast and slow wind (e.g., D’Amicis et al. 2019b).

## 6. DISCUSSION

It is well-known that Alfvénic turbulence is anisotropic, its properties dependent on the angle,  $\theta_{kB}$ . For a single spacecraft sampling in time, the common assumption of ergodicity means that we measure a statistically similar distribution of turbulent fluctuations. Hence, by sampling along different directions relative to a changing  $\theta_{vB}$ , we measure different components of the same distribution, e.g., the spectrum of magnetic fluctuations parallel and perpendicular to



**Figure 4.** (a) Median proton perpendicular temperature,  $T_{p,\perp}/\langle T_{p,\perp} \rangle$  and (b) median proton parallel temperature,  $T_{p,\parallel}/\langle T_{p,\parallel} \rangle$ , across  $\beta_p$ - $\theta_{vB}$  space. In both panels, we column-normalise the data by the median temperature in each  $\beta_p$  bin,  $\langle T_{p,\perp/\parallel} \rangle$ , to remove the systematic dependency of  $\beta_p$  on temperature. The dashed black lines indicate the isocontours of  $\bar{\sigma}_m(\theta_{vB}) = 0$  mirrored about the line  $\theta_{vB} = 90^\circ$ . We also include contours of constant  $\sigma_\perp = 0.3$  from Figure 3(b) as black lines.

$\mathbf{B}_0$ . The same is true for magnetic helicity, where the left- or right-handedness is determined only by the sampling direction. Certain fluctuations may still exist and we do not measure them since we do not sample close enough to the  $\mathbf{k}$  of these modes for them to make a significant contribution to the  $\mathbf{k} \cdot \mathbf{v}_{sw}$  term in Equation 9. Therefore, if turbulent dissipation is ongoing, we expect the resultant heating to exhibit the same distribution as the fluctuations at ion-kinetic scales. This is because the polarisation properties of solar wind fluctuations affect what dissipation mechanisms can occur.

We initially hypothesised that the proton temperature would not exhibit a systematic dependence on either  $\theta_{vB}$  or  $\sigma_{\perp,\parallel}$ . However, we show a clear dependence of  $T_{p,\perp/\parallel}/\langle T_{p,\perp/\parallel} \rangle$  on  $\theta_{vB}$  in Figure 4 that also correlates with the magnetic helicity signatures of different Alfvénic fluctuations at ion-kinetic scales. This result suggests that the properties of the turbulence also change with  $\theta_{vB}$ . In other words, differences in the spectra of magnetic fluctuations with changing  $\theta_{vB}$  are due to both single-spacecraft sampling effects and differences in the underlying distribution of turbulent fluctuations. If this interpretation is correct, studies that sample many angles  $\theta_{vB}$  as the solar wind flows past a single spacecraft to build up a picture of the turbulence in the plasma, i.e., to sample different  $\theta_{kB}$ , need to be interpreted very carefully (e.g., Horbury et al. 2008;

Wicks et al. 2010; He et al. 2011; Podesta & Gary 2011b). In this study, we measure  $\theta_{vB}$  at  $\sim 92$  s timescales, which suppresses large-scale correlations such as the Parker-spiral. Instead, we show correlations between small-scale fluctuations with respect to a local mean field and the macroscopic proton temperature. Therefore, it is fair to assume that the dependence of  $T_{p,\perp}/\langle T_{p,\perp} \rangle$  and  $T_{p,\parallel}/\langle T_{p,\parallel} \rangle$  on  $\theta_{vB}$  and  $\beta_p$  reflects the differences in the localised dissipation and heating processes at ion-kinetic scales in the solar wind.

A large enough  $T_{p,\perp}/T_{p,\parallel}$  can drive AIC waves unstable in the solar wind (Kasper et al. 2002b; Matteini et al. 2007; Bale et al. 2009; Maruca et al. 2012). The driving of these waves is enhanced by the frequent presence of an  $\alpha$ -particle proton differential flow or proton beam in the solar wind (Podesta & Gary 2011a,b; Wicks et al. 2016; Woodham et al. 2019; Zhao et al. 2019b, 2020a). The enhancement in  $T_{p,\perp}/\langle T_{p,\perp} \rangle$  at quasi-parallel angles in Figure 4(a) is likely responsible for the driving of these modes and correlates with the peak in  $\sigma_\parallel$  at these angles in Figure 3(a), where we measure the strongest signal. While we are unable to observe AIC waves at oblique angles using a single spacecraft, we also measure KAW-like fluctuations at these angles using  $\sigma_\perp$  in Figure 3(b). The peaks in  $\sigma_\perp$  correlate with the observed enhancement in  $T_{p,\perp}/\langle T_{p,\perp} \rangle$ , and therefore, are consistent with the dissipation of these fluctuations leading to perpendicular heating. A common dissipation mechanism proposed for KAW-like fluctuations is Landau damping (e.g., Howes 2008; Schekochihin et al. 2009); however, this leads to heating parallel to  $\mathbf{B}_0$ . Instead, perpendicular heating may arise from processes such as stochastic heating (Chandran et al. 2010, 2013) or even cyclotron resonance (Isenberg & Vasquez 2019), although more work is needed to confirm this.

We note that several studies (Markovskii & Vasquez 2013, 2016; Markovskii et al. 2016; Vasquez et al. 2018) show that non-linear fluctuations confined to the plane perpendicular to  $\mathbf{B}_0$  can produce the observed right-handed helicity signature in  $\sigma_\perp$  in the same way as linear KAWs (e.g., Howes & Quataert 2010; He et al. 2012b). In this study, we refer to KAW-like fluctuations as non-linear turbulent fluctuations with polarisation properties that are consistent with linear KAWs, rather than linear modes. This interpretation does not preclude the possibility of resonant damping (Li et al. 2016, 2019; Klein et al. 2017a, 2020; Howes et al. 2018; Chen et al. 2019) or stochastic heating (e.g., Cerri et al. 2021) discussed above, however, additional processes cannot be ruled out. For example, kinetic simulations show perpendicular heating of ions by turbulent processes that may be unrelated to wave damping or stochastic heating, although, the exact heating mechanism is still unclear (e.g., Parashar et al. 2009; Servidio et al. 2012; Vasquez 2015; Yang et al. 2017).

The variation of  $T_{p,\parallel}/\langle T_{p,\parallel} \rangle$  in the  $\beta_p$ - $\theta_{vB}$  plane in Figure 4(b) is more difficult to interpret. This result could also be a signature of proton Landau damping of KAW-like fluctuations, although, this process is typically stronger at  $\beta_p \gtrsim 1$  (Gary & Nishimura 2004; Kawazura et al. 2019). While we measure fluctuations that can consistently explain the enhancement in  $T_{p,\parallel}/\langle T_{p,\parallel} \rangle$ , other fluctuations may be present that we do not measure. Direct evidence of energy transfer between the fluctuations and protons is needed to confirm this result, for example, using the field-particle correlation method (Klein & Howes 2016; Howes et al. 2017; Klein 2017; Klein et al. 2017b; Chen et al. 2019; Li et al. 2019). This evidence will require higher-resolution data than provided by *Wind*. We



note that caution must be given when interpreting these results, since several other effects may also explain the temperature dependence seen in the  $\beta_p$ - $\theta_{vB}$  plane. For example, instrumental effects and the role of solar wind expansion may result in similar temperature profiles. We now discuss these two effects in turn, showing that they cannot fully replicate our results presented in this paper.

## 7. ANALYSIS CAVEATS

### 7.1. Instrumentation & Measurement Uncertainties

The SWE Faraday cups on-board *Wind* measure a reduced VDF that is a function of the average direction of  $\mathbf{B}_0$  over the measurement interval (Kasper 2002). As the spacecraft spins every 3 s in the ecliptic plane, the Faraday cups measure the current due to ions in several angular windows. The Faraday cups repeat this process using a different voltage (energy) window for each spacecraft rotation, building up a full spectrum every  $\sim 92$  s. By fitting a bi-Maxwellian to the reduced proton VDF, the proton thermal speeds,  $w_{p,\parallel}$  and  $w_{p,\perp}$ , are obtained and converted to temperatures via  $T_{p,\perp/\parallel} = m_p w_{p,\perp/\parallel}^2 / 2k_B$ , where  $m_p$  is the proton mass. Due to the orientation of the cups on the spacecraft body, the direction of  $\mathbf{B}_0$  with respect to the axis of the cups as they integrate over the proton VDF can cause inherent uncertainty in  $w_{p,\parallel}$  and  $w_{p,\perp}$ . For example, if  $\mathbf{B}_0$  is radial, then measurements of  $w_{p,\parallel}$  have a smaller uncertainty compared to when the field is perpendicular to the cup, i.e.,  $\mathbf{B}_0$  is orientated out of the ecliptic plane by a significant angle,  $\theta_{vB} \gtrsim 60^\circ$  (Kasper et al. 2006). In Figure 5, we plot the percentage uncertainty in  $w_{p,\parallel}$  and  $w_{p,\perp}$ ,

$$U(w_{p,\perp/\parallel}) = \frac{\Delta w_{p,\perp/\parallel}}{w_{p,\perp/\parallel}} \times 100\%, \quad (19)$$

in the  $\beta_p$ - $\theta_{vB}$  plane, where  $\Delta w_{p,\perp/\parallel}$  is the uncertainty in  $w_{p,\perp/\parallel}$ , derived from the non-linear fitting of the distribution functions. We note that these uncertainties are not equivalent to Gaussian measurement errors; however, they provide a qualitative aid to understand systematic instrumental issues in the Faraday cup data.

We see that  $w_{p,\perp}$  has a larger uncertainty ( $\sim 40\%$ ) at quasi-parallel angles in Figure 5(a), which is almost independent of  $\beta_p$ . While the median  $T_{p,\perp}/\langle T_{p,\perp} \rangle$  in Figure 4(a) is larger at these angles, it exhibits a clear dependence on  $\beta_p$ . Therefore, increased uncertainty in the temperature measurements alone cannot completely account for the observed enhancement in  $T_{p,\perp}/\langle T_{p,\perp} \rangle$  at these angles in the  $\beta_p$ - $\theta_{vB}$  plane. At quasi-perpendicular angles, the uncertainty in  $w_{p,\perp}$  is less than 10%, suggesting that the enhancements in  $T_{p,\perp}/\langle T_{p,\perp} \rangle$  in Figure 4(a) at  $\beta_p \simeq 1$  and  $40^\circ \lesssim \theta_{vB} \lesssim 140^\circ$  are unlikely to result from instrumental uncertainties. From Figure 5(b), the uncertainty in  $w_{p,\parallel}$  is largest at  $\theta_{vB} \simeq 90^\circ$ , although there is a larger spread to  $70^\circ \lesssim \theta_{vB} \lesssim 110^\circ$  at  $\beta_p \gtrsim 0.3$ . By comparing with Figure 4(b), the enhancement in  $T_{p,\parallel}/\langle T_{p,\parallel} \rangle$  over the entire  $\beta_p$  range does not coincide exactly with the regions of  $\beta_p$ - $\theta_{vB}$  space where these measurements have increased uncertainty. We also expect that any increased uncertainty in the  $w_{p,\parallel}$  measurements would lead to increased noise that destroys any coherent median signal in this space, weakening the enhancement seen in Figure 4(b). Therefore, we conclude that the increased uncertainty in  $w_{p,\parallel}$  at oblique angles is not the sole cause of the observed enhancement in  $T_{p,\parallel}/\langle T_{p,\parallel} \rangle$ .

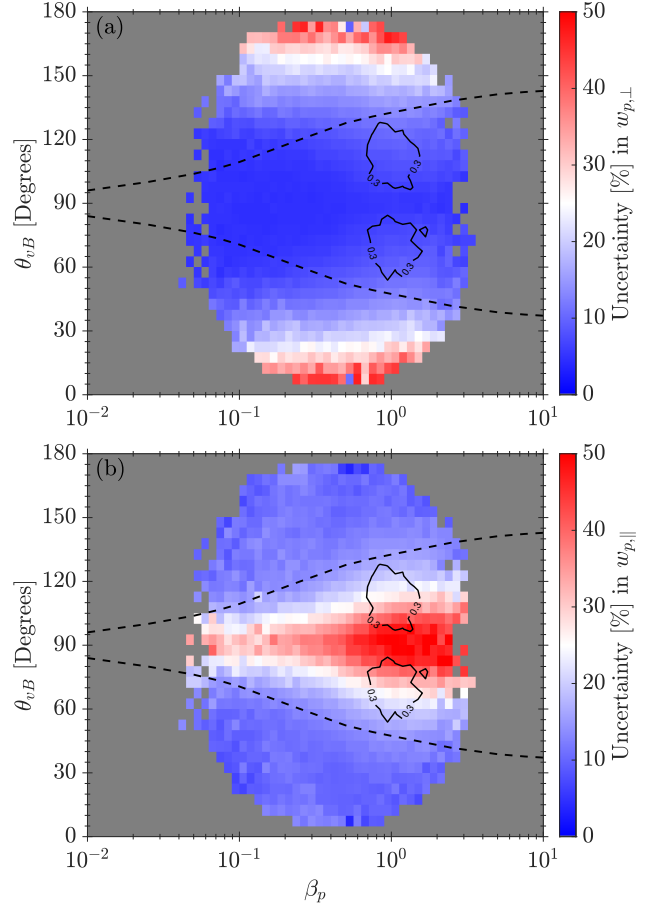


**Figure 5.** Median percentage uncertainty in (a)  $w_{p,\perp}$  and (b)  $w_{p,\parallel}$ , across  $\beta_p$ - $\theta_{vB}$  space. The dashed black lines indicate the isocontours of  $\bar{\sigma}_m(\theta_{vB}) = 0$  mirrored about the line  $\theta_{vB} = 90^\circ$ . We also include contours of constant  $\sigma_{\perp} = 0.3$  from Figure 3(b) as black lines.

Another source of uncertainty from the SWE measurements arises from the changing magnetic field direction over the course of the  $\sim 92$  s measurement interval (Maruca & Kasper 2013). We quantify the angular fluctuations in  $\mathbf{B}$  using:

$$\psi_B = \sum_{i=1}^N \arccos(\hat{\mathbf{B}}_i \cdot \hat{\mathbf{B}}_{92}) / N, \quad (20)$$

where  $N$  is the number of spacecraft rotations in a single measurement,  $\hat{\mathbf{B}}_{92}$  is the average magnetic field direction over the whole measurement interval, and  $\hat{\mathbf{B}}_i$  is the magnetic field unit vector averaged over each 3 s rotation. A large  $\psi_B$  can lead to the blurring of anisotropies in the proton thermal speeds. In other words, the fluctuations in  $\mathbf{B}$  over the integration time result in a broadening of the reduced VDFs, increasing uncertainty in these measurements (e.g., see Verscharen & Marsch 2011). To reduce this blurring effect, we remove SWE measurements with angular deviations  $\psi_B > 15^\circ$ . Maruca (2012) provides an alternative dataset of proton moments from SWE measurements to account for large deviations in the instantaneous magnetic field, using an average  $\mathbf{B}_0$  over each voltage window scan (i.e., one rotation of the spacecraft,  $\sim 3$  s) to calculate  $w_{p,\perp}$  and  $w_{p,\parallel}$ . Maruca & Kasper (2013) show that the Kasper (2002) dataset often underestimates the temperature anisotropy of proton VDFs. Our comparison with this alternative dataset (not shown here) reveals that both  $T_{p,\perp}/\langle T_{p,\perp} \rangle$

711 and  $T_{p,\parallel}/\langle T_{p,\parallel} \rangle$  show a similar, albeit slightly reduced, dependence  
 712 on both  $\beta_p$  and  $\theta_{vB}$ . This result suggests that the  
 713 temperature dependence we see in the  $\beta_p$ - $\theta_{vB}$  plane is unlikely  
 714 caused by the blurring of proton temperature anisotropy mea-  
 715 surements.

### 7.2. CGL Spherical Expansion

716  
 717 Another possible source of proton temperature dependence  
 718 on  $\theta_{vB}$  is the expansion of the solar wind as it flows out into the  
 719 heliosphere. The double adiabatic closure presented by Chew  
 720 et al. (1956) predicts the evolution of  $T_{p,\perp}$  and  $T_{p,\parallel}$  assuming  
 721 no collisions, negligible heat flux, and no local heating:

$$\frac{d}{dt} \left( \frac{T_{p,\perp}}{B} \right) = 0 \quad \text{and} \quad \frac{d}{dt} \left( \frac{T_{p,\parallel} B^2}{n_p^2} \right) = 0, \quad (21)$$

722 where  $d/dt$  is the convective derivative. Under the assump-  
 723 tion of steady-state spherical expansion, which is purely trans-  
 724 verse to the radial direction with a constant radial velocity,  
 725  $\mathbf{v}_{sw} = v_{sw} \hat{\mathbf{R}}$ , the continuity equation gives  $n_p \propto 1/r^2$ , where  $r$   
 726 is the radial distance from the Sun. We assume that the radial  
 727 evolution of the magnetic field in the equatorial plane follows  
 728 the Parker spiral (Parker 1958),

$$B \propto \frac{\sqrt{\cos^2 \phi_0 + r^2 \sin^2 \phi_0}}{r^2}, \quad (22)$$

729 which gives a radial dependence of  $B \propto 1/r^2$  when  $\phi_0 = 0^\circ$   
 730 and  $B \propto 1/r$  when  $\phi_0 = 90^\circ$ . The angle,  $\phi_0$ , is the foot-point  
 731 longitude of the field at the solar wind source surface, given  
 732 by:

$$\phi_0 = \arctan \left( \frac{r_0 \Omega_\odot}{v_{sw}} \right), \quad (23)$$

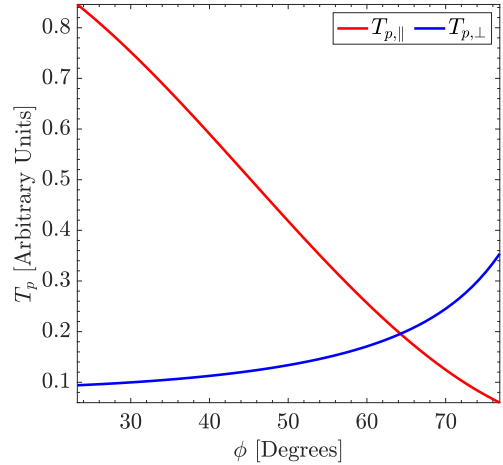
733 where  $\Omega_\odot = 2.85 \times 10^{-6}$  rad/s is the constant solar angular  
 734 rotation rate and  $r_0 \simeq 20R_\odot$  (Owens & Forsyth 2013). There-  
 735 fore, a value of  $v_{sw}$  sets the value of  $\phi_0$  at a given radius,  
 736  $r_0$ . Then,  $\phi = \tan^{-1}(B_\phi/B_r)$  is the azimuthal angle of  $\mathbf{B}$   
 737 in the equatorial plane at a distance,  $r$ , from the Sun. The two  
 738 angles are related by  $\tan \phi = R \tan \phi_0$ , where  $R = r/r_0$ . From  
 739 Equations 21, 22, and the radial dependence of  $n_p$ , we obtain:

$$\frac{T_{p,\perp}}{T_{0,\perp}} = \frac{\sqrt{\cos^2(\phi_0) + R^2 \sin^2(\phi_0)}}{R^2}, \quad (24)$$

740 and

$$\frac{T_{p,\parallel}}{T_{0,\parallel}} = \frac{1}{\cos^2(\phi_0) + R^2 \sin^2(\phi_0)}, \quad (25)$$

743 where  $T_{0,\perp}$  and  $T_{0,\parallel}$  are the perpendicular and parallel proton  
 744 temperatures at  $r_0$ , respectively. We use Equations 24 and 25  
 745 to investigate the dependence of proton temperature on  $\phi$  at  
 746  $r = 215R_\odot \simeq 1$  au. Since the solar wind velocity is radial, the  
 747 angle  $\phi$  is approximately equal to  $\theta_{vB}$ . We set  $T_{0,\perp} = 10$  and  
 748  $T_{0,\parallel} = 1$ , giving  $R = 10.75$  for  $r_0 = 20R_\odot$ . We create a distri-  
 749 bution of angles  $\phi_0$  using Equation 23 by selecting a range of  
 750 wind speeds:  $100 \leq v_{sw} \leq 1000$  km/s. This range of  $\phi_0$  gives  
 751  $20^\circ \lesssim \phi \lesssim 80^\circ$  at 1 au. In Figure 6, we show the variation of  
 752  $T_{p,\perp}$  and  $T_{p,\parallel}$  with  $\phi$ . We choose a larger  $T_{\perp,0}$  to show more



753 **Figure 6.** The temperature profiles  $T_{p,\parallel}$  and  $T_{p,\perp}$  as functions of  $\phi$  at  $r \simeq 1$   
 754 au for CGL spherical expansion given by Equations 24 and 25.

755 clearly the variation in  $T_{p,\perp}$ . We see that  $T_{p,\parallel}$  remains simi-  
 756 lar to the value set close to the Sun (small  $\phi$ ), and decreases  
 757 rapidly with increasing  $\phi$ , approaching zero at  $\phi \gtrsim 70^\circ$ . On  
 758 the other hand,  $T_{p,\perp}$  is largest at  $\phi \gtrsim 60^\circ$  and approaches 0.1  
 759 for  $\phi \lesssim 30^\circ$ . This dependence of  $T_{p,\perp}$  and  $T_{p,\parallel}$  is opposite to  
 760 what we observe in Figure 4, which in general shows larger  
 761  $T_{p,\parallel}$  at  $\theta_{vB} \simeq 90^\circ$  and larger  $T_{p,\perp}$  at  $\theta_{vB} \simeq 0^\circ$ . Therefore, spheri-  
 762 cal expansion alone cannot explain our results.

## 8. CONCLUSIONS

763 We use magnetic helicity to investigate the polarisation  
 764 properties of Alfvénic fluctuations with finite radial wave-  
 765 number,  $k_r$ , at ion-kinetic scales in the solar wind. Using  
 766 almost 15 years of *Wind* observations, we separate the contri-  
 767 butions to helicity from fluctuations with wave-vectors quasi-  
 768 parallel and oblique to  $\mathbf{B}_0$ , finding that the helicity of Alfvénic  
 769 fluctuations is consistent with predictions from linear Vlasov  
 770 theory. In particular, the peak in magnetic helicity at ion-  
 771 kinetic scales and its variation with  $\beta_p$  and  $\theta_{vB}$  shown in Fig-  
 772 ure 3 are in agreement with the dispersion relation of linear  
 773 Alfvén waves (Gary 1986), when modified by Taylor’s hypo-  
 774 thesis. This result suggests that the non-linear turbulent  
 775 fluctuations at these scales share at least some polarisation  
 776 properties with Alfvén waves.

777 We also investigate the dependence of local kinetic heat-  
 778 ing processes due to turbulent dissipation on  $\theta_{vB}$ . In Figure  
 779 4, we find that both  $T_{p,\perp}$  and  $T_{p,\parallel}$ , when normalised to their  
 780 average value in each  $\beta_p$ -bin, show a clear dependence on  
 781  $\theta_{vB}$ . The temperature parallel to  $\mathbf{B}_0$  is generally higher in  
 782 the parameter-space where we measure a coherent helicity signa-  
 783 ture associated with KAW-like fluctuations, and perpendicular  
 784 temperature higher in the parameter-space where we measure  
 785 a signature expected from AIC waves. We also see small en-  
 786 hancements in the perpendicular temperature where we mea-  
 787 sure the strongest helicity signal of KAW-like fluctuations.  
 788 However, we re-iterate the important fact that the lack of a  
 789 wave signal is not the same as a lack of presence of waves.

790 Our results suggest that the properties of turbulent fluctua-  
 791 tions at ion-kinetic scales in the solar wind depends on the an-  
 792 gle  $\theta_{vB}$ . This finding is inconsistent with the general assump-  
 793 tion that sampling different  $\theta_{vB}$  allows us to sample different  
 794 parts of the same ensemble of fluctuations that is otherwise  
 795 unaltered in its statistical properties. Therefore, studies that  
 796 sample different  $\theta_{vB}$  in order to sample different  $\theta_{kB}$  need to be

796 interpreted very carefully. Instead, if we assume that the dis-  
 797 sipation mechanisms and proton heating depend on  $\theta_{vB}$ , the  
 798 enhancements in proton temperature in Figure 4 are consis-  
 799 tent with the role of wave-particle interactions in determining  
 800 proton temperature in the solar wind. For example, whenever  
 801 we measure the helicity of AIC waves or KAW fluctuations,  
 802 then we also measure enhancements in proton temperature.  
 803 However, the inverse is not necessarily true. We suggest that  
 804 heating mechanisms associated with KAWs lead to both paral-  
 805 lel (Howes 2008; Schekochihin et al. 2009) and perpendic-  
 806 ular (Chandran et al. 2010, 2013; Isenberg & Vasquez 2019)  
 807 heating. We rule out both instrumental and large-scale expan-  
 808 sion effects, finding that neither of them alone can explain the  
 809 observed temperature profile in the  $\beta_p$ - $\theta_{vB}$  plane.

810 In summary, our observations suggest that the properties of  
 811 Alfvénic fluctuations at ion-kinetic scales determine the level  
 812 of proton heating from turbulent dissipation. This interpre-  
 813 tation is consistent with recent studies showing that larger  
 814 magnetic helicity signatures at ion-kinetic scales are associ-  
 815 ated with larger proton temperatures and steeper spectral ex-  
 816 ponents (Pine et al. 2020; Zhao et al. 2020b, 2021). Our find-  
 817 ings, therefore, provide new evidence for the importance of  
 818 local kinetic processes in determining proton temperature in  
 819 the solar wind. We emphasise that our conclusions do not in-  
 820 voke causality, just correlation. For example, we cannot rule  
 821 out a lack of cooling rather than heating. However, while the  
 822 adiabatic expansion of the solar wind causes the temperature  
 823 to vary with  $\theta_{vB}$ , this cannot explain the observed temperature  
 824 profiles in the  $\beta_p$ - $\theta_{vB}$  plane. Further work is ongoing in order  
 825 to confirm these results and develop a theory for the processes  
 826 associated with the polarisation properties of Alfvénic fluctu-  
 827 ations that lead to the observed temperature profiles.

828 LDW thanks B. Alterman, L. Matteini, D. Stansby, and  
 829 J. Stawarz for useful comments and discussions. LDW is  
 830 also grateful to B. Maruca for sharing his processed SWE  
 831 dataset for validation testing. LDW was supported by an  
 832 STFC studentship at UCL/MSSL ST/N504488/1 and the  
 833 STFC consolidated grant ST/S000364/1 to Imperial Col-  
 834 lege London; DV was supported by STFC Ernest Ruther-  
 835 ford Fellowship ST/P003826/1; RTW was supported by the  
 836 STFC consolidated grants to UCL/MSSL, ST/N000722/1 and  
 837 ST/S000240/1. JMT was supported by NSF SHINE award  
 838 (AGS-1622306). GGH was supported by NASA grants  
 839 80NSSC18K1217 and 80NSSC18K0643. All data from the  
 840 *Wind* spacecraft used in this study are publicly available and  
 841 were obtained from the NASA [SPDF web-site](https://github.com/danielver02/NHDS). The NHDS  
 842 code is available at <https://github.com/danielver02/NHDS>.

#### 843 APPENDIX

##### 844 DECOMPOSITION OF FLUCTUATING MAGNETIC HELICITY

845 Here we present a mathematical derivation that decomposes  
 846  $\sigma_m^r(k_r)$  into the different contributions,  $\sigma_{ij}^r(k_i)$ , calculated us-  
 847 ing Equation 13 (see also Wicks et al. 2012). In Figure 7, we  
 848 plot the median value of the peak in  $\sigma_m^r(k_r)$  across the  $\beta_p$ - $\theta_{vB}$   
 849 plane, showing two helicity signatures of opposite handed-  
 850 ness. This technique allows us to separate the helicity signa-  
 851 tures of different fluctuations at ion-kinetic scales in the solar  
 852 wind, as we show in Figure 3.

853 We consider a spacecraft that samples a single mode with  
 854 wave-vector:

$$\mathbf{k} = k_{\perp} \cos \alpha \hat{\mathbf{x}} + k_{\perp} \sin \alpha \hat{\mathbf{y}} + k_{\parallel} \hat{\mathbf{z}}, \quad (\text{A1})$$

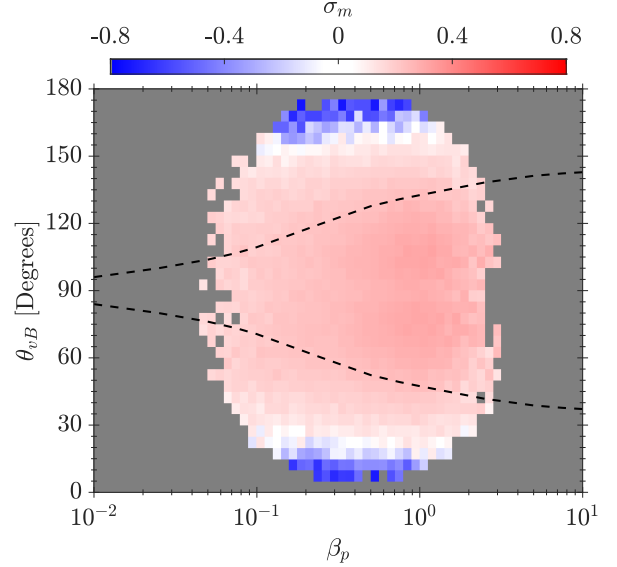


**Figure 7.** Median value of the peak in  $\sigma_m^r(k_r)$  across the  $\beta_p$ - $\theta_{vB}$  plane. The dashed black lines indicate the isocontours of  $\bar{\sigma}_m(\theta_{vB}) = 0$  mirrored about the line  $\theta_{vB} = 90^\circ$ .

where  $\alpha$  is the azimuthal angle of  $\mathbf{k}$  in the  $x$ - $y$  plane. The full signal from turbulence corresponds to a superposition of the signals from each of the modes, so considering a single mode is sufficient to understand how the components  $\sigma_{ij}^r(k_i)$  are related to  $\sigma_m^r(k_r)$ . Without loss of generality, we take the solar wind velocity to be in the  $x$ - $z$  plane,

$$\mathbf{v}_{sw} = v_{sw} \sin \theta_{vB} \hat{\mathbf{x}} + v_{sw} \cos \theta_{vB} \hat{\mathbf{z}}, \quad (\text{A2})$$

and the local mean magnetic field to be  $\mathbf{B}_0 = B_0 \hat{\mathbf{z}}$ . We use the relation  $2\text{Im}\{a^*b\} \equiv i(ab^* - a^*b)$  to rewrite  $H_m^r(k_r)$  in RTN coordinates from Equation 7 into the form:

$$H_m^r(k_r) = i \frac{\delta B_T \delta B_N^* - \delta B_T^* \delta B_N}{k_r}. \quad (\text{A3})$$

The normalised reduced fluctuating magnetic helicity,  $\sigma_m^r(k_r)$ , is then given by Equation 11. We define the relation between the RTN and the field-aligned (Equation 12) coordinate systems using the unit vector along the sampling direction,  $\hat{\mathbf{v}}_{sw} = \mathbf{v}_{sw}/|\mathbf{v}_{sw}|$ :

$$\begin{aligned} \hat{\mathbf{R}} &= \hat{\mathbf{v}}_{sw} = \sin \theta_{vB} \hat{\mathbf{x}} + \cos \theta_{vB} \hat{\mathbf{z}}; \\ \hat{\mathbf{T}} &= \hat{\mathbf{B}}_0 \times \hat{\mathbf{v}}_{sw} / |\hat{\mathbf{B}}_0 \times \hat{\mathbf{v}}_{sw}| = \hat{\mathbf{y}}; \\ \hat{\mathbf{N}} &= \hat{\mathbf{R}} \times \hat{\mathbf{T}} = -\cos \theta_{vB} \hat{\mathbf{x}} + \sin \theta_{vB} \hat{\mathbf{z}}. \end{aligned} \quad (\text{A4})$$

By substituting for the RTN unit vectors in terms of  $\hat{\mathbf{x}}$ ,  $\hat{\mathbf{y}}$ , and  $\hat{\mathbf{z}}$  and simplifying, we obtain:

$$\begin{aligned} \sigma_m^r(k_r) = \frac{1}{|\delta \mathbf{B}(k_r)|^2} \left\{ \left[ \frac{i(\delta B_x \delta B_y^* - \delta B_x^* \delta B_y)}{k_z} \right] k_z \cos \theta_{vB} \right. \\ + \left[ \frac{i(\delta B_x \delta B_z^* - \delta B_x^* \delta B_z)}{k_y} \right] k_y \sin \theta_{vB} \sin \alpha \\ \left. + \left[ \frac{i(\delta B_y \delta B_z^* - \delta B_y^* \delta B_z)}{k_x} \right] k_x \sin \theta_{vB} \cos \alpha \right\}. \end{aligned} \quad (\text{A5})$$

871 By defining the non-reduced fluctuating magnetic helicity  
872 (see also, Equation 5) as:

$$\begin{aligned} H'_m(\mathbf{k}) &= i \frac{\delta B_x \delta B_y^* - \delta B_x^* \delta B_y}{k_z} \\ &\equiv i \frac{\delta B_y \delta B_z^* - \delta B_y^* \delta B_z}{k_x} \equiv i \frac{\delta B_z \delta B_x^* - \delta B_z^* \delta B_x}{k_y}, \end{aligned} \quad (\text{A6})$$

873 we can manipulate Equation A5 into the form,

$$\begin{aligned} \sigma_m^r(k_r) &= \frac{H'_m(\mathbf{k})}{|\delta \mathbf{B}(k_r)|^2} \{k_z \cos \theta_{vB} - k_y \sin \theta_{vB} \sin \alpha \\ &\quad + k_x \sin \theta_{vB} \cos \alpha\}, \\ &\equiv \sigma_{xy}(k_z) \cos \theta_{vB} + \sigma_{xz}(k_y) \sin \theta_{vB} \sin \alpha \\ &\quad + \sigma_{yz}(k_x) \sin \theta_{vB} \cos \alpha, \end{aligned} \quad (\text{A7})$$

874 where we define the different contributions,  $\sigma_{ij}(k_l)$ , using  
875 Equation 13. We equate each of the terms between the two  
876 forms in Equation A7 to obtain the following direct relations  
877 between  $\sigma_m^r(k_r)$  and  $\sigma_{xy}(k_z)$ ,  $\sigma_{xz}(k_y)$  and  $\sigma_{yz}(k_x)$ :

$$\sigma_{xy}(k_z) = \frac{H'_m(\mathbf{k})}{|\delta \mathbf{B}(k_r)|^2} k_z = \sigma_m^r(k_r) \frac{k_z}{k_r}, \quad (\text{A8})$$

$$\sigma_{xz}(k_y) = -\frac{H'_m(\mathbf{k})}{|\delta \mathbf{B}(k_r)|^2} k_y = -\sigma_m^r(k_r) \frac{k_y}{k_r}, \quad (\text{A9})$$

878 and,

$$\sigma_{yz}(k_x) = \frac{H'_m(\mathbf{k})}{|\delta \mathbf{B}(k_r)|^2} k_x = \sigma_m^r(k_r) \frac{k_x}{k_r}, \quad (\text{A10})$$

879 which are the same as Equations 14, 15, and 16.

880 To highlight the separation of different fluctuations in the  
881 solar wind using this technique, we show in Figure 8(a) a time  
882 series of magnetic helicity spectra,  $\sigma_m^r$ , measured by *Wind*  
883 on 01/07/2012. We plot the spectra as functions of frequency in  
884 the spacecraft frame,  $f_{sc} = \omega_{sc}/2\pi$  (see Equation 10). In panels  
885 (b)-(d), we also plot  $\sigma_{ij}$ , showing the decomposition of  
886  $\sigma_m^r$  into its three components. The two coherent signatures  
887 of opposite handedness at  $f_{sc} \simeq 1$  Hz in panel (a) are completely  
888 separated into the components  $\sigma_{xy}$  and  $\sigma_{yz}$  in panels  
889 (b) and (c). In panel (d), we see only small enhancements  
890 close to 0.33 Hz, which corresponds to the spin frequency of  
891 the spacecraft. Besides this spacecraft artefact, there is no coherent  
892 helicity signature in  $\sigma_{xz}$ , as expected.

## REFERENCES

893 Alexandrova, O., Chen, C. H. K., Sorriso-Valvo, L., Horbury, T. S., & Bale,  
894 S. D. 2013, *Space Science Reviews*, 178, 101 1  
895 Alfvén, H. 1942, *Nature*, 150, 405 2  
896 Alterman, B. L., Kasper, J. C., Stevens, M. L., & Koval, A. 2018, *The*  
897 *Astrophysical Journal*, 864, 112 1  
898 Bale, S. D., Kasper, J. C., Howes, G. G., et al. 2009, *Physical Review*  
899 *Letters*, 103, 211101 1, 5, 5, 6  
900 Bale, S. D., Kellogg, P. J., Mozer, F. S., Horbury, T. S., & Reme, H. 2005,  
901 *Physical Review Letters*, 94, 215002 1, 5  
902 Barnes, A. 1981, *Journal of Geophysical Research*, 86, 7498 1  
903 Batchelor, G. K. 1970, *The Theory of Homogenous Turbulence* (Cambridge  
904 University Press) 3

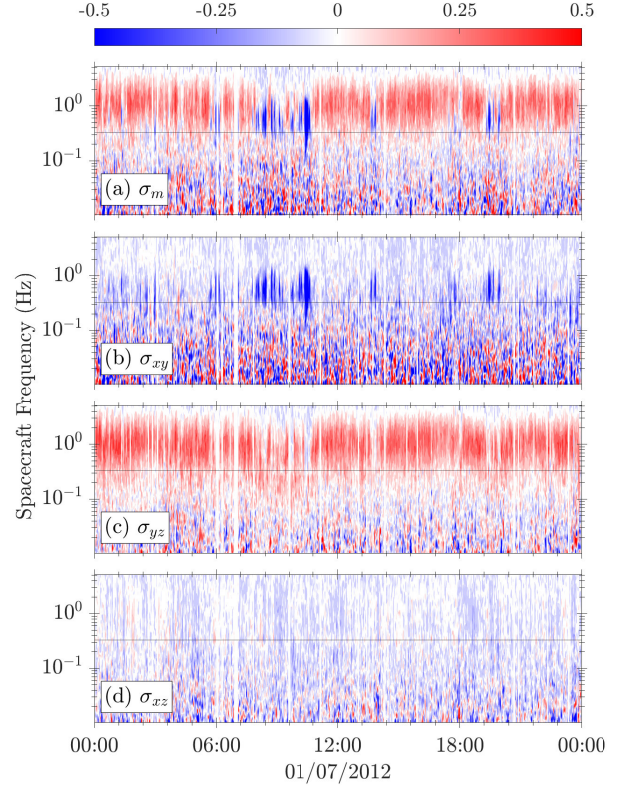


**Figure 8.** (a) Time series of reduced normalised fluctuating magnetic helicity spectra,  $\sigma_m^r$ , for a day of observations on 01/07/2012. The different contributions to the total helicity, (b)  $\sigma_{xy}$ , (c)  $\sigma_{yz}$ , and (d)  $\sigma_{xz}$ , respectively. We plot the spectra as functions of the frequency in the spacecraft frame,  $f_{sc} = \omega_{sc}/2\pi$ . The black dashed line in panel (d) is the spacecraft spin frequency, 0.33 Hz.

905 Belcher, J. W., & Davis Jr., L. 1971, *Journal of Geophysical Research*, 76,  
906 3534 1  
907 Belcher, J. W., Davis Jr., L., & Smith, E. J. 1969, *Journal of Geophysical*  
908 *Research*, 74, 2302 1  
909 Boldyrev, S., & Perez, J. C. 2012, *The Astrophysical Journal*, 758, L44 1  
910 Bourouaine, S., Marsch, E., & Neubauer, F. M. 2010, *Geophysical Research*  
911 *Letters*, 37, 1 1  
912 Bourouaine, S., Verscharen, D., Chandran, B. D., Maruca, B. A., & Kasper,  
913 J. C. 2013, *Astrophysical Journal Letters*, 777, L3 1  
914 Bruno, R., & Carbone, V. 2013, *Living Reviews in Solar Physics*, 10, 2 1  
915 Bruno, R., & Telloni, D. 2015, *The Astrophysical Journal Letters*, 811, L17  
916 3  
917 Cerri, S. S., Arzamaskey, L., & Kunz, M. W. 2021, *arXiv: 2102.09654*, The  
918 *Astrophysical Journal*, submitted 6  
919 Chandran, B. D. G., Li, B., Rogers, B. N., Quataert, E., & Germaschewski,  
920 K. 2010, *The Astrophysical Journal*, 720, 503 1, 6, 8  
921 Chandran, B. D. G., Verscharen, D., Quataert, E., et al. 2013, *The*  
922 *Astrophysical Journal*, 776, 45 1, 6, 8  
923 Chen, C. H. K. 2016, *Journal of Plasma Physics*, 82 1  
924 Chen, C. H. K., Klein, K. G., & Howes, G. G. 2019, *Nature*  
925 *Communications*, 10, 740 6  
926 Chen, C. H. K., Mallet, A., Schekochihin, A. A., et al. 2012, *The*  
927 *Astrophysical Journal*, 758, 120 1  
928 Chen, C. H. K., Mallet, A., Yousef, T. A., Schekochihin, A. A., & Horbury,  
929 T. S. 2011, *Monthly Notices of the Royal Astronomical Society*, 415,  
930 3219 1  
931 Chew, G. F., Goldberger, M. L., & Low, F. E. 1956, *Proceedings of the*  
932 *Royal Society A: Mathematical and Physical Sciences*, 236 1, 7.2  
933 Coleman, P. J. 1968, *The Astrophysical Journal*, 153, 371 1  
934 D'Amicis, R., & Bruno, R. 2015, *The Astrophysical Journal*, 805, 84 4  
935 D'Amicis, R., De Marco, R., Bruno, R., & Perrone, D. 2019a, *Astronomy &*  
936 *Astrophysics*, 632, A92 1  
937 D'Amicis, R., Matteini, L., & Bruno, R. 2019b, *Monthly Notices of the*  
938 *Royal Astronomical Society*, 483, 4665 4, 5  
939 Forman, M. A., Wicks, R. T., & Horbury, T. S. 2011, *The Astrophysical*  
940 *Journal*, 733, 76 3

- 941 Fredricks, R. W., & Coroniti, F. V. 1976, *Journal of Geophysical Research*, 81, 5591 3
- 942
- 943 Galtier, S. 2006, *Journal of Plasma Physics*, 72, 721 1
- 944 Galtier, S., & Buchlin, E. 2007, *The Astrophysical Journal*, 656, 560 1
- 945 Gary, S. P. 1986, *Journal of Plasma Physics*, 35, 431 2, 8
- 946 —. 1993, *Theory of Space Plasma Microinstabilities* (Cambridge University Press) 2
- 947
- 948 Gary, S. P., & Borovsky, J. E. 2004, *Journal of Geophysical Research: Space Physics*, 109, A06105 2
- 949
- 950 Gary, S. P., Jian, L. K., Broiles, T. W., et al. 2015, *Journal of Geophysical Research: Space Physics*, 121, 30 1
- 951
- 952 Gary, S. P., & Nishimura, K. 2004, *Journal of Geophysical Research: Space Physics*, 109, A02109 2, 6
- 953
- 954 He, J., Marsch, E., Tu, C., Yao, S., & Tian, H. 2011, *Astrophysical Journal*, 731, 85 1, 3, 4, 6
- 955
- 956 He, J., Tu, C., Marsch, E., & Yao, S. 2012a, *Astrophysical Journal Letters*, 745, L8 3
- 957
- 958 —. 2012b, *Astrophysical Journal*, 749, 86 3, 6
- 959
- 960 Hellinger, P., & Trávníček, P. M. 2014, *Astrophysical Journal Letters*, 784, L15 5
- 961
- 962 Hellinger, P., Trávníček, P. M., Kasper, J. C., & Lazarus, A. J. 2006, *Geophysical Research Letters*, 33, L09101 1
- 963
- 964 Horbury, T. S., Forman, M. A., & Oughton, S. 2008, *Physical Review Letters*, 101, 175005 1, 3, 4, 6
- 965
- 966 Horbury, T. S., Matteini, L., & Stansby, D. 2018, *Monthly Notices of the Royal Astronomical Society*, 478, 1980 1
- 967
- 968 Howes, G. G. 2008, *Physics of Plasmas*, 15, 6, 8
- 969
- 970 Howes, G. G., Bale, S. D., Klein, K. G., et al. 2012, *Astrophysical Journal Letters*, 753, 2 1
- 971
- 972 Howes, G. G., Dorland, W., Cowley, S. C., et al. 2006, *The Astrophysical Journal*, 651, 590 1
- 973
- 974 Howes, G. G., Dorland, W., Cowley, S. C., et al. 2008, *Physical Review Letters*, 100, 065004 1, 5
- 975
- 976 Howes, G. G., Klein, K. G., & Li, T. C. 2017 6
- 977
- 978 Howes, G. G., Klein, K. G., & Tenbarga, J. M. 2014, *The Astrophysical Journal*, 789, 106 3
- 979
- 980 Howes, G. G., McCubbin, A. J., & Klein, K. S. G. 2018, *Journal of Plasma Physics*, 84, 905840105 6
- 981
- 982 Howes, G. G., & Quataert, E. 2010, *The Astrophysical Journal Letters*, 709, L49 2, 6
- 983
- 984 Isenberg, P. A., & Vasquez, B. J. 2019, *The Astrophysical Journal*, 887, 63 1, 6, 8
- 985
- 986 Kasper, J. C. 2002, PhD thesis, Massachusetts Institute of Technology 7.1, 7.1
- 987
- 988 Kasper, J. C., Lazarus, A. J., & Gary, S. P. 2002a, *Geophysical Research Letters*, 29, 1839 1
- 989
- 990 —. 2002b, *Geophysical Research Letters*, 29, 20 5, 6
- 991
- 992 —. 2008, *Physical Review Letters*, 101, 261103 1
- 993
- 994 Kasper, J. C., Lazarus, A. J., Steinberg, J. T., Ogilvie, K. W., & Szabo, A. 2006, *Journal of Geophysical Research: Space Physics*, 111, A03105 4, 7.1
- 995
- 996 Kasper, J. C., Maruca, B. A., Stevens, M. L., & Zaslavsky, A. 2013, *Physical Review Letters*, 110, 091102 1
- 997
- 998 Kasper, J. C., Klein, K. G., Weber, T., et al. 2017, *The Astrophysical Journal*, 849, 126 1, 4
- 999
- 1000 Kawazura, Y., Barnes, M., & Schekochihin, A. A. 2019, *Proceedings of the National Academy of Sciences of the United States of America*, 116, 771 6
- 1001
- 1002 Klein, K. G. 2017, *Physics of Plasmas*, 24 6
- 1003
- 1004 Klein, K. G., Alterman, B. L., Stevens, M. L., Vech, D., & Kasper, J. C. 2018, *Physical Review Letters*, 120, 205102 1
- 1005
- 1006 Klein, K. G., & Howes, G. G. 2015, *Physics of Plasmas*, 22, 032903 1
- 1007
- 1008 —. 2016, *The Astrophysical Journal Letters*, 826, L30 6
- 1009
- 1010 Klein, K. G., Howes, G. G., & TenBarge, J. M. 2014a, *The Astrophysical Journal Letters*, 790, L20 3
- 1011
- 1012 —. 2017a, *Journal of Plasma Physics*, 83, 535830401 6
- 1013
- 1014 —. 2017b, *Journal of Plasma Physics*, 83, 1 6
- 1015
- 1016 Klein, K. G., Howes, G. G., Tenbarga, J. M., et al. 2012, *Astrophysical Journal*, 755 1
- 1017
- 1018 Klein, K. G., Howes, G. G., TenBarge, J. M., & Podesta, J. J. 2014b, *The Astrophysical Journal*, 785, 138 3
- 1019
- 1020 Klein, K. G., Howes, G. G., Tenbarga, J. M., & Valentini, F. 2020, *Journal of Plasma Physics*, 86, 905860402 6
- 1021
- 1022 Klein, K. G., Martinović, M., Stansby, D., & Horbury, T. S. 2019, *The Astrophysical Journal*, 887, 234 1, 2
- 1023
- 1024 Koval, A., & Szabo, A. 2013, in *AIP Conference Proceedings*, Vol. 1539, 211 4
- 1025
- 1026 Leamon, R. J., Smith, C. W., Ness, N. F., & Wong, H. K. 1999, *Journal of Geophysical Research: Space Physics*, 104, 22331 1, 5
- 1027
- 1028 Lepping, R. P., Acuña, M. H., Burlaga, L. F., et al. 1995, *Space Science Reviews*, 71, 207 4
- 1029
- 1030 Li, T. C., Howes, G. G., Klein, K. G., Liu, Y.-H., & TenBarge, J. M. 2019, *Journal of Plasma Physics*, 85, 905850406 6
- 1031
- 1032 Li, T. C., Howes, G. G., Klein, K. G., & TenBarge, J. M. 2016, *The Astrophysical Journal Letters*, 832, L24 6
- 1033
- 1034 MacBride, B. T., Smith, C. W., & Vasquez, B. J. 2010, *Journal of Geophysical Research: Space Physics*, 115 1
- 1035
- 1036 Markovskii, S. A., & Vasquez, B. J. 2013, *The Astrophysical Journal*, 768, 62 6
- 1037
- 1038 —. 2016, *The Astrophysical Journal*, 820, 15 6
- 1039
- 1040 Markovskii, S. A., Vasquez, B. J., & Smith, C. W. 2016, *The Astrophysical Journal*, 833, 212 6
- 1041
- 1042 Marsch, E. 2006, *Living Reviews in Solar Physics*, 3, 1 1
- 1043
- 1044 —. 2012, *Space Science Reviews*, 172, 23 1
- 1045
- 1046 Marsch, E., Goertz, C. K., & Richter, K. 1982, *Journal of Geophysical Research*, 87, 5030 1
- 1047
- 1048 Marsch, E., Vocks, C., & Tu, C. Y. 2003, *Nonlinear Processes in Geophysics*, 10, 101 1
- 1049
- 1050 Maruca, B. 2012, PhD thesis, Harvard University 7.1
- 1051
- 1052 Maruca, B. A., Bale, S. D., Sorriso-Valvo, L., Kasper, J. C., & Stevens, M. L. 2013, *Physical Review Letters*, 111, 241101 1, 4
- 1053
- 1054 Maruca, B. A., & Kasper, J. C. 2013, *Advances in Space Research*, 52, 723 7.1, 7.1
- 1055
- 1056 Maruca, B. A., Kasper, J. C., & Bale, S. D. 2011, *Physical Review Letters*, 107, 1 5
- 1057
- 1058 Maruca, B. A., Kasper, J. C., & Gary, S. P. 2012, *The Astrophysical Journal*, 748, 137 1, 5, 6
- 1059
- 1060 Matteini, L., Hellinger, P., Landi, S., Trávníček, P. M., & Velli, M. 2012, *Space Science Reviews*, 172, 373 1
- 1061
- 1062 Matteini, L., Horbury, T. S., Neugebauer, M., & Goldstein, B. E. 2014, *Geophysical Research Letters*, 41, 259 1
- 1063
- 1064 Matteini, L., Horbury, T. S., Pantellini, F., Velli, M., & Schwartz, S. J. 2015, *Astrophysical Journal*, 802, 11 1
- 1065
- 1066 Matteini, L., Landi, S., Hellinger, P., et al. 2007, *Geophysical Research Letters*, 34, L20105 1, 5, 6
- 1067
- 1068 Matthaeus, W. H., Elliott, H. A., & McComas, D. J. 2006, *Journal of Geophysical Research: Space Physics*, 111, A10103 5
- 1069
- 1070 Matthaeus, W. H., & Goldstein, M. L. 1982a, *Journal of Geophysical Research*, 87, 6011 4
- 1071
- 1072 —. 1982b, *Journal of Geophysical Research*, 87, 10,347 2, 3
- 1073
- 1074 Matthaeus, W. H., Goldstein, M. L., & Smith, C. W. 1982, *Physical Review Letters*, 48, 1256 2, 3
- 1075
- 1076 Montgomery, M. D., & Turner, L. 1981, *Physics of Fluids*, 24, 825 3
- 1077
- 1078 Ogilvie, K. W., Chornay, D. J., Fritzenreiter, R. J., et al. 1995, *Space Science Reviews*, 71, 55 4
- 1079
- 1080 Osman, K. T., Matthaeus, W. H., Hnat, B., & Chapman, S. C. 2012, *Physical Review Letters*, 108, 261103 5
- 1081
- 1082 Owens, M. J., & Forsyth, R. J. 2013, *Living Reviews in Solar Physics*, 10 7.2
- 1083
- 1084 Parashar, T. N., Shay, M. A., Cassak, P. A., & Matthaeus, W. H. 2009, *Physics of Plasmas*, 16, arXiv:0801.0107 6
- 1085
- 1086 Parker, E. N. 1958, *The Astrophysical Journal*, 128, 664 7.2
- 1087
- 1088 Perri, S., & Balogh, A. 2010, *The Astrophysical Journal*, 714, 937 3
- 1089
- 1090 Perri, S., Goldstein, M. L., Dorelli, J. C., & Sahrhoui, F. 2012, *Physical Review Letters*, 109, 1 1
- 1091
- 1092 Perrone, D., D'Amicis, R., De Marco, R., et al. 2020, *Astronomy & Astrophysics*, 633, A166 4
- 1093
- 1094 Perrone, D., Stansby, D., Horbury, T. S., & Matteini, L. 2019, *Monthly Notices of the Royal Astronomical Society*, 488, 2380 5
- 1095
- 1096 Pine, Z. B., Smith, C. W., Hollick, S. J., et al. 2020, *The Astrophysical Journal*, 900, 91 8
- 1097
- 1098 Podesta, J. J., & Gary, S. P. 2011a, *The Astrophysical Journal*, 742, 41 6
- 1099
- 1100 —. 2011b, *The Astrophysical Journal*, 734, 15 1, 3, 4, 6
- 1101
- 1102 Šafránková, J., Němeček, Z., Němec, F., et al. 2019, *The Astrophysical Journal*, 870, 40 1
- 1103
- 1104 Sahrhoui, F., Goldstein, M. L., Belmont, G., Canu, P., & Rezeau, L. 2010, *Physical Review Letters*, 105, 131101 1, 5
- 1105
- 1106 Schekochihin, A. A., Cowley, S. C., Dorland, W., et al. 2009, *The Astrophysical Journal Supplement Series*, 182, 310 1, 6, 8
- 1107
- 1108 Servidio, S., Valentini, F., Califano, F., & Veltri, P. 2012, *Physical Review Letters*, 108, 1 6
- 1109
- 1110 Stansby, D., Horbury, T. S., & Matteini, L. 2019, *Monthly Notices of the Royal Astronomical Society*, 482, 1706 4

- 1094 Stix, T. H. 1992, *Waves in Plasmas* (American Institute of Physics) [2, 2](#)
- 1095 Sundkvist, D., Retinò, A., Vaivads, A., & Bale, S. D. 2007, *Physical Review Letters*, [99, 1 1](#)
- 1096 Taylor, G. I. 1938, *Proceedings of the Royal Society A: Mathematical and Physical Sciences*, [164, 476 3](#)
- 1098 Telsoni, D., & Bruno, R. 2016, *Monthly Notices of the Royal Astronomical Society: Letters*, [463, L79 3](#)
- 1100 Telsoni, D., Bruno, R., & Trenchi, L. 2015, *The Astrophysical Journal*, [805, 46 3](#)
- 1102 Torrence, C., & Compo, G. P. 1998, *Bulletin of the American Meteorological Society*, [79, 61 4](#)
- 1104 Tu, C. Y., & Marsch, E. 1995, *Space Science Reviews*, [73, 1 1](#)
- 1105 Vasquez, B. J. 2015, *Astrophysical Journal*, [806, 33 6](#)
- 1106 Vasquez, B. J., Markovskii, S. A., & Smith, C. W. 2018, *The Astrophysical Journal*, [855, 121 6](#)
- 1108 Verscharen, D., Bourouaine, S., Chandran, B. D., & Maruca, B. A. 2013, *Astrophysical Journal*, [773 2](#)
- 1109 Verscharen, D., & Chandran, B. D. G. 2018, *Research Notes of the AAS*, [2, 13 2](#)
- 1111 Verscharen, D., Klein, K. G., & Maruca, B. A. 2019, *Living Reviews in Solar Physics*, [16, 5 1](#)
- 1114 Verscharen, D., & Marsch, E. 2011, *Annales Geophysicae*, [29, 909 7.1](#)
- 1115 Wicks, R. T., Forman, M. A., Horbury, T. S., & Oughton, S. 2012, *The Astrophysical Journal*, [746, 103 3, 3, A](#)
- 1118 Wicks, R. T., Horbury, T. S., Chen, C. H. K., & Schekochihin, A. A. 2010, *Monthly Notices of the Royal Astronomical Society*, [407, L31 1, 3, 4, 6](#)
- 1119 Wicks, R. T., Alexander, R. L., Stevens, M. L., et al. 2016, *The Astrophysical Journal*, [819, 6 6](#)
- 1120 Wicks, R. T., Stevens, M. L., Kasper, J. C., et al. 2018, *The Astrophysical Journal Supplement Series*, [236, 41 4](#)
- 1121 Woltjer, L. 1958a, *Proceedings of the National Academy of Sciences*, [44, 489 2](#)
- 1122 —. 1958b, *Proceedings of the National Academy of Sciences*, [44, 833 2](#)
- 1123 Woodham, L. D., Wicks, R. T., Verscharen, D., & Owen, C. J. 2018, *The Astrophysical Journal*, [856, 49 4, 5](#)
- 1124 Woodham, L. D., Wicks, R. T., Verscharen, D., et al. 2019, *The Astrophysical Journal Letters*, [884, L53 1, 3, 3, 4, 4, 5, 5, 6](#)
- 1125 Yang, Y., Matthaeus, W. H., Parashar, T. N., et al. 2017, *Physics of Plasmas*, [24, 072306 6](#)
- 1126 Zhao, G. Q., Feng, H. Q., Wu, D. J., et al. 2020a, *The Astrophysical Journal Letters*, [889, L14 6](#)
- 1127 —. 2018, *Journal of Geophysical Research: Space Physics*, [123, 1715 5](#)
- 1128 Zhao, G. Q., Feng, H. Q., Wu, D. J., Pi, G., & Huang, J. 2019a, *The Astrophysical Journal*, [871, 175 5](#)
- 1129 Zhao, G. Q., Li, H., Feng, H. Q., et al. 2019b, *The Astrophysical Journal*, [884, 60 6](#)
- 1130 Zhao, G. Q., Lin, Y., Wang, X. Y., et al. 2021, *The Astrophysical Journal*, [906, 123 8](#)
- 1131 —. 2020b, *Geophysical Research Letters*, [47, 1 8](#)